Retrieval of Venus' cloud parameters from VIRTIS **nightside** spectra in the latitude band 25°-55°N

Davide Magurno[a,1,*], Tiziano Maestri[a], Davide Grassi[b], Giuseppe Piccioni[b], Giuseppe Sindoni[b]

[a] *Department of Physics and Astronomy, University of Bologna, viale Carlo Berti Pichat 6/2, 40127, Bologna, Italy*
[b] *INAF-IAPS, via del Fosso del Cavaliere 100, 00133, Roma, Italy*

Abstract

Two years of data from the M-channel of the Visible and InfraRed Thermal Imaging Spectrometer (VIRTIS), on-board of the European Space Agency mission Venus Express operating around the Venus planet, are analysed. Nocturnal data from a nadir viewpoint in the latitude band 25°N-55°N are selected for their configuration advantages and maximisation of the scene homogeneity. A reference model, and radiance spectrum, is defined based on average accepted values of the Venus main atmospheric and clouds parameters found in the literature. Extensive radiative transfer simulations are performed to provide a synthetic database of more than 10 000 VIRTIS radiances representing the natural variability of the system parameters (atmospheric temperature profile, cloud H_2O-H_2SO_4 solution concentration and

*Corresponding author
Email addresses: davide.magurno@roma2.infn.it (Davide Magurno), tiziano.maestri@unibo.it (Tiziano Maestri), davide.grassi@iaps.inaf.it (Davide Grassi), giuseppe.piccioni@iaps.inaf.it (Giuseppe Piccioni), giuseppe.sindoni@iaps.inaf.it (Giuseppe Sindoni)
[1]Present Address: *Department of Physics, University of Roma Tor Vergata, via Della Ricerca Scientifica 1, 00133, Roma, Italy*

vertical distribution, particle size distribution density and modal radius). A simulated-observed fitting algorithm of spectral radiances in windows channels, based on a weighting procedure accounting for the latitudinal observed radiance variations, is used to derive the best atmosphere-cloud configuration for each observation.

Results show that the reference Venus model does not adequately reproduce the observed VIRTIS spectra. In particular, the model accounting for a constant sulphuric acid concentration along the vertical extent is never selected as a best fit. The 75%/96% and 84%/96% concentrations (the first values refer to the upper cloud layers and the second values to the lower ones) are the most commonly retrieved models representing more than 85% of the retrieved cases for any latitudinal band considered. It is shown that the stratified concentration of aqueous sulphuric acid assumption allows to adequately fit the observed radiance, in particular the peak at 1.74 µm and around 4 µm.

The analysis of the results concerning the microphysics suggests larger radii for the uppermost cloud layers in conjunction with a large reduction of their number density with respect to the reference standard. Considerable variations of the particle concentrations in the Venus' atmosphere are retrieved for altitudes between 60 and 70 km. The retrieved models also suggest that lowest cloud layers have smaller particles radii and larger number density than expected from the reference model. Latitudinal variations of microphysical and chemical parameters are also analysed.

Keywords: Venus, VIRTIS, Clouds, Radiative transfer, Chemical composition

---

1. Introduction

The current knowledge of the nature and properties of the Venus' aerosols derives from a variety of sources, including ground based observations, satellite remote sensing and in situ measurements by entry probes and balloons. In particular, data from the Pioneer probe nephelometer were fundamental to depict the overall scenario that is still considered valid today (Knollenberg and Hunten, 1980). From space to surface, we first meet a population of submicron haze, detected yet at about 100 km. A second micron-size component shows up below 70 km. This is the main constituent, in terms of mass, of the upper clouds of Venus and has a large impact on what is typically observed from space at visible and infrared (IR) wavelengths. A local minimum in cloud opacity at about 57 km marks the transition to what is considered the middle/lower cloud deck, where larger particles are found. The altitude of 48 km shows a sharp decrease in aerosol opacity, and below only optically thinner diffuse haze and spotted clouds of uncertain nature can be found (e.g. Grieger et al., 2003). In situ analysis (Hoffman et al., 1980), as well as remote IR (Zasova et al., 2007) and polarimetric measurements (Hansen and Hovenier, 1974) have allowed to identify a liquid mixture of sulphuric acid and water as the main constituent of haze and upper clouds. Consistently, the clearing observed at the altitude of 48 km is met where Venus' environmental temperature allows the sulphuric acid to evaporate Krasnopolsky and Pollack (1994). Other components fill the atmosphere as well: UV observations show high contrasting details, demonstrating the existence of a still unidentified UV absorber, strongly variable in space and time (e.g. Markiewicz et al., 2007); the VEGA balloon instruments clearly suggest the

presence of Chlorine, Phosphorus and Iron in unknown components of the deeper clouds (Andreichikov et al., 1987).

The long observation campaign of Venus Express from 2006 to 2014 represents a milestone in the exploration of the Venus' atmosphere. The large suite of instruments operating from thermal IR (5 µm) to UV enables a series of studies, mostly focused on upper clouds and hazes. Several efforts have been performed and some are resumed in what follows. The studies of latitudinal trends in upper clouds heights and scale heights by Ignatiev et al. (2009), Lee et al. (2012) and Haus et al. (2014) from VIRTIS nadir data demonstrated that both parameters decrease poleward from about 50° in latitude. The sun occultation measurements by SPICAV/SOIR (Wilquet et al., 2012) demonstrated that haze presents occasionally detached layers (also found by SPICAV/IR, Luginin et al., 2014) and that also haze is characterized by a bi-modal size distribution, making therefore weaker the distinction between haze and upper clouds. A recent study of phase functions derived from VMC nadir observations by Shalygina et al. (2015) shows that sub-micron particles are preferentially found on the morning hemisphere and highlighted an increase of refractive index in the region between 40°S and 60°S, as well as a slight increase of the size for the so-called "mode 2"population toward the poles (a conclusion also found by Wilson et al., 2008).

The main objective of the present study is to provide a statistical retrieval of the Venus' clouds chemical and microphysical properties by exploiting VIRTIS data in the nadir viewing geometry. Some previous studies on clouds analysis based on VIRTIS data focused on the Venus' southern hemisphere (e.g. Barstow et al., 2012; Haus et al., 2014)**; however, the pixel foot-**

print of the instrument is smaller over the northern hemisphere, so that it is expected that the atmospheric variability within a single pixel is also smaller and a more detailed analysis can be performed. Nighttime data are necessary to avoid the solar scattering, that would completely mask the deep clouds spectral features. VIRTIS data are then compared with a large synthetic dataset of spectral radiances computed with DISORT on the modelled atmosphere and clouds. The new approach on the clouds modelling is to consider them as vertically non-uniform in sulphuric acid concentration instead of a homogeneous layer as usually done (e.g. Zasova et al., 2007; Bézard et al., 2011).

A short overview of the instrument is given in Section 2. In Section 3 we explore the data archive and data selection. Section 4 defines the initial model for the Venus' atmosphere. Some sensitivity analysis is performed in Section 5. In Section 6 and 7 we define the parameters for the creation of a synthetic dataset and the fitting of observed data with the synthetic ones. The dataset analysis is performed in Section 8. Finally, the conclusions are presented in Section 9.

2. VIRTIS on Venus Express

The Visible and InfraRed Thermal Imaging Spectrometer (VIRTIS) is a diffraction spectrometer on-board Venus Express (VEx), a mission of the European Space Agency (ESA) operating around the Venus planet from 2006 until the end of 2014. The orbit was highly elliptical, near-polar, 24 hours, with the pericentre located between 80°N and 90°N at about 250 km altitude and the apocentre located approximately 66 000 km above the surface. The

Venus Express mission is based on the opportunity to re-fly a spare model of the Mars Express spacecraft and some related payload. In addition, a spare model of the precursor VIRTIS instrument devoted to study the comet 67P/Churyumov-Gerasimenko, has been adapted ad hoc for the Venus environment and then included in the core payloads of VEx. VIRTIS operated in the spectral range from UV to thermal IR in two separated optics, named VIRTIS-M and VIRTIS-H (Piccioni et al., 2007; Erard, 2012). VIRTIS-M had high resolution imaging capability at moderate spectral resolution in the range between 0.25 µm and 5.2 µm. It was in turn divided into two channels, M-VIS from 0.25 µm to 1 µm and M-IR from 1 µm to 5.2 µm. VIRTIS-H had high spectral resolution in the range between 2 µm and 5 µm but without imaging capability. This work focuses on data collected by VIRTIS-M IR. One of the main parameters affecting observations is the exposure time, that can change from 0.02 s to 18 s. The majority of nocturnal observations has an exposure time of 3.3 s for long-lasting observations or 0.36 s for the briefest ones. The advantage in long-lasting records is the high SNR, the disadvantage is the loss of information for wavelengths longer than about 4 µm since the detector is saturated by the thermal background (Piccioni et al., 2007).

3. Data archive selection

The archive of VIRTIS-M IR data consists of a set of measurements collected in 517 orbits performed from 11/04/2006 to 27/10/2008 (after this date the M-channel of the instrument turned off). Each orbit is divided into sub-sections, called *cubes*, characterised by uniform conditions of observation, such as the same exposure time and pointing mode. The total number

of available cubes is 4537 all over the planet, each of them storing from less than 10 to more than 100 000 individual spectra. Only part of the whole dataset is selected in accordance with the following specific observing conditions. a) Observations above the northern hemisphere, where the orbit is closer to the surface, have a relatively small pixel footprint at nadir. The spatial resolution is about 190 m at 45°N, given that the observation altitude is at around 760 km. Therefore, the observed pixel area is expected to be more homogeneous than in the southern hemisphere. b) Nocturnal observations give more information about the entire vertical extent of the clouds, because the atmospheric radiance is not masked by the solar reflected component. c) **Nadir-looking of the instrument is accounted for, limiting the pointing angle to values between 0 degree and 1 degree off-nadir.** In others words, we assume that the upper limit for nadir viewing is 1 degree. These conditions reduce the dataset to only 90 cubes regarding 90 different days spanning over the whole lifetime mission. The useful observations are strongly reduced with respect to the initial database since the majority of nadir observations were taken in the southern hemisphere. To carry out a statistical analysis of the nadir dataset an additional selection is performed, excluding the data outside the latitude band between 25°N and 55°N. This choice allows to maintain a small pixel footprint and to avoid possible interactions with peculiar atmospheric phenomena such as the cold collar (60-80°N) and the hot dipole (75-85°N) (Zasova et al., 2007; Piccioni et al., 2007). The final selection accounts for a total number of 65 cubes.

As a consequence of the near polar orbit, all the cubes have a similar structure for nadir observations: a very narrow scan in longitude (the max-

imum width is about 0.8 degrees) but extended in latitude from the north pole to the equator (Figure 1, left panel). Therefore, atmospheric changes are mainly visible as meridional variations, looking as horizontally homogeneous radiance stripes in the images. Observations are then grouped in $0.2^\circ \times 0.2^\circ$ grid of latitude $\times$ longitude (about 21 km $\times$ 16 km footprint at 40°N). For each bin, it is assumed that the measured radiance is representative of an homogeneous scene. The choice of the bin size has been made after testing the latitudinal/longitudinal variation of radiance from one pixel to another. Figure 2 shows an example of radiance variation versus latitude. The latitudinal difference between the two groups of data is about 0.7°. A sensible radiance difference is noticed between the two groups, whereas only small changes are observed along the longitude (as also noticed from the left panel of Figure 1). Radiance measured at specific wavelengths shows, in some cases, evident outliers mainly due to cosmic rays, ionising radiation or electrical surges. They look like isolated peaks in the spectrum with very high absolute values, both positive and negative. To remove these outliers, the Chauvenet's criterion is applied to each bin at every wavelength. After the outliers removal, data within each bin are finally averaged and standard deviations are calculated to obtain a single representative value for each bin.

The final useful dataset is thus reduced to 11 383 bins from a total of 115 795 observations distributed in three latitude bands: 25-35°N, 35-45°N, 45-55°N. These spectra (band representative) are then analysed to retrieve clouds properties.

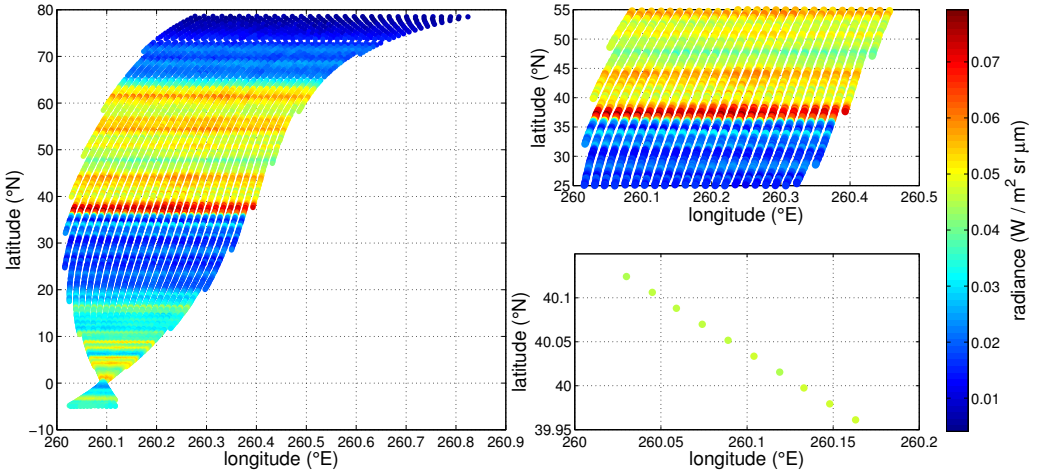

Figure 1: Example of data selection for the cube VI0097_19 (27/07/2006). Each dot corresponds to a single observation. Plotted radiances are measured at 2.3 µm, the colorbar on the right provides the radiance intensity. Left: all the nocturnal nadir observations of the cube are shown. Top right: observations in the latitude band 25-55°N. Bottom right: one of the selected bins of 0.2°×0.2°.

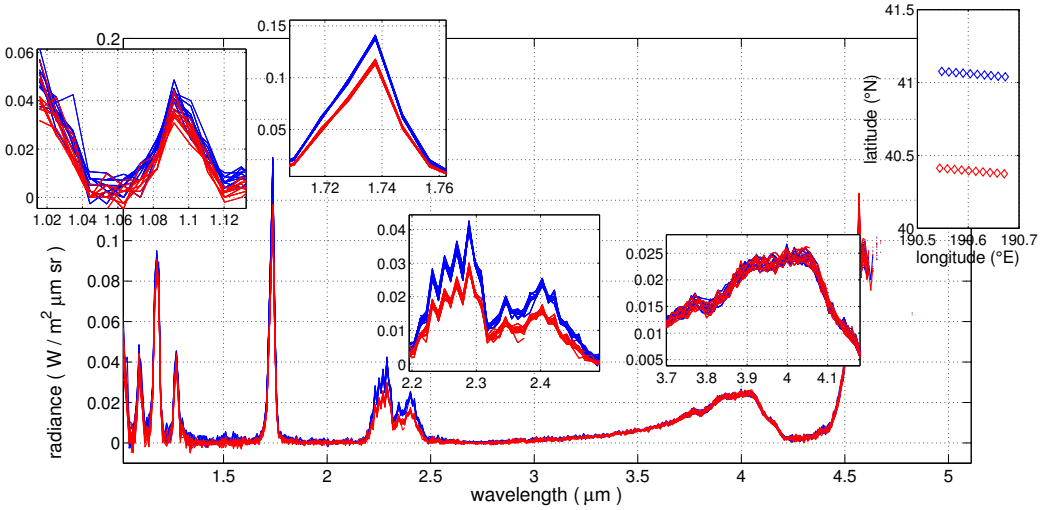

Figure 2: 20 observations from the cube VI0901_03 (08/10/2008). Half of total observations are collected at latitudes close to 40.5°N (in red) and half close to 41°N (in blue) as shown in the top-right inset panel. The differences at the 1.74 µm and 2.3 µm windows are zoomed out. Measured radiances are almost identical near 1 µm and at 4 µm as highlighted in the inset panels.

4. Venus 'Reference' model

In this Section we provide the radiative transfer modelling details and define the so-called reference condition for the Venus' atmosphere. The standard Venus is the one that represents the state-of-the-art in the present knowledge and modelling. We focus on clouds and atmospheric parameters. One of the goal of our analysis is, in fact, to highlight possible differences in the retrieval parameters from what is usually assumed in literature and possibly define a more accurate description of the Venus' clouds.

4.1. Modelling of the gas component

Temperature and pressure profiles of the Venus' atmosphere were initially defined as standard profiles in the eighties, then revised over the years. These standard profiles are known as the Venus International Reference Atmosphere (VIRA) and describe the atmosphere of Venus from the ground up to 100 km altitude with a vertical resolution of 1-2 km (Kliore et al., 1985; Seiff et al., 1985; Moroz and Zasova, 1997; Zasova, 2012). Due to the large thermal inertia and almost adiabatic conditions of the lower atmosphere, the VIRA profiles below 30 km are assumed to be the same independently of planet's latitude and longitude. Above 30 km the profiles show meridional variability and are defined for five latitudes: 30, 45, 60, 75 and 85 degrees (mentioned as VIRA 30, VIRA 45, etc. in the text), with small differences in pressure. VIRA 30 and VIRA 45 are taken into account in this study. A comparison of these two temperature profiles shows lower temperatures in the altitude range 55-70 km and higher ones from 70 to 90 km for the VIRA 45. The top of the atmosphere (TOA) is set at 100 km altitude in the models, since

the observed radiance comes almost entirely from layers below that altitude with the exception of few narrow spectral bands that are particularly opaque.

The gases concentration profiles are dominated by the presence of carbon dioxide molecules. A constant value for CO_2 of about 96.5% by volume is assumed. For the principal minor constituents which are optically active in the VIRTIS 1-5 µm band we refer to Haus and Arnold (2010), who suggest the vertical profiles of Volume Mixing Ratios (VMR) shown in Figure 3 for H_2O, CO, SO_2, OCS, HCl and HF, from the ground up to 100 km. About 3.5% by volume of the Venus' atmosphere is composed of N_2, that has no absorption in the analysed spectral band and so it is only considered for molecular scattering. In addition to these gases, the Venus' atmosphere has many other compounds (Esposito et al., 1997; de Bergh et al., 2006; Mills et al., 2007; Krasnopolsky, 2012) but their VMR are rather small and their interaction with radiation, between 1 and 5 µm, is sufficiently weak to make them negligible for the present radiative transfer computations. Spectroscopic properties of gases are retrieved from multiple databases. The most popular one is HITRAN (Rothman et al., 2013) that is undoubtedly the main available database to describe the Earth's atmosphere for nadir viewing simulations. Nevertheless, the HITRAN database shows some limits when applied to the Venus' atmosphere. Some energetic transitions are neglected in the Earth's typical conditions since they are too weak and totally unimportant when simulating upwelling radiances. In many cases, these transitions assume importance in the radiative transfer computations when the high temperatures and pressures of the Venus case are accounted for. Therefore,

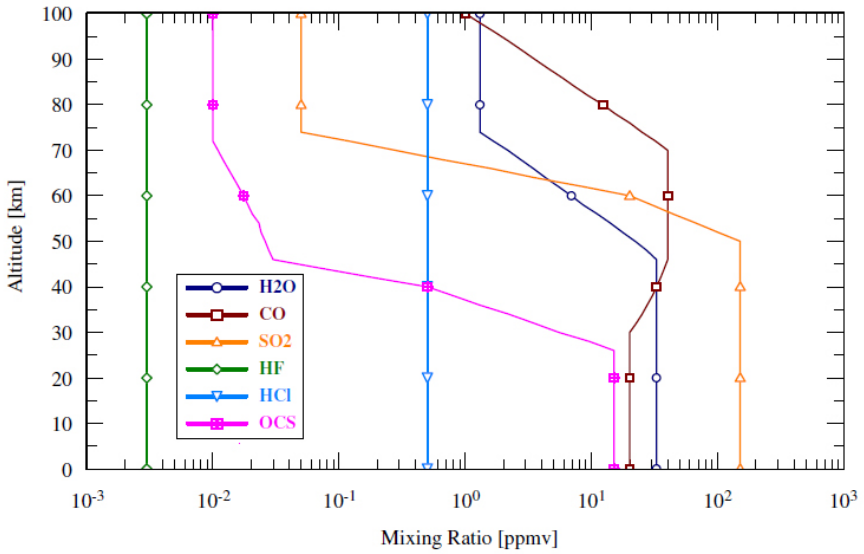

Figure 3: Volume mixing ratio profiles of the main minor constituents of the Venus' atmosphere (from Haus and Arnold, 2010).

specific databases have been created to include the weakest transition of the main Venusian gases. The two databases used for this purpose are HITEMP (Rothman et al., 2010) and HOTBASE (Pollack et al., 1993). HITEMP has been specifically developed to overpass the limitations of HITRAN as it provides energetic transition parameters at temperatures higher than 400 K for five gas species: H_2O, CO_2, CO, NO and OH. HOTBASE is a specific database for CO_2, developed for the Venus' atmosphere. This database, usable at high temperatures, takes into account some minor absorption lines of CO_2 that are missing in HITEMP (Bézard et al., 2011). Exploiting the three database strengths, our choice is to use HOTBASE for CO_2, HITEMP for H_2O and CO, HITRAN for SO_2, OCS, HCl and HF.

ARS (Ignatiev et al., 2005) is a suite of codes implementing line-by-line calculations of gaseous and aerosol optical depth and atmospheric radiance spectra. In this work, ARS is used to compute the absorption coefficients of the gases which have an active role in the Venus' atmosphere in the 1-5 µm band. To considerably reduce the computation time, referring to Haus and Arnold (2010), the spectral lines weaker than 10^{-28} cm^{-1}/(molecules cm^{-2}) are removed for each gas except CO_2, which is extended to 10^{-35} cm^{-1}/(molecules cm^{-2}). The discarded lines are sufficiently weak to be negligible in the final result. A regular grid for the computation is chosen with a 0.02 cm^{-1} step between 2000 cm^{-1} and 10000 cm^{-1}, so that the whole VIRTIS-M IR range is represented at high resolution. The Voigt profile defined by Kuntz (1997) is selected as line shape. The absorption line cut-off is taken from Haus et al. (2013) and set equal to 125 cm^{-1} for each gas except CO_2. For CO_2, a differential cut-off depending on wavenumber is used: 125 cm^{-1} from 2000 cm^{-1} to 7500 cm^{-1} and 250 cm^{-1} from 7500 cm^{-1} to 10000 cm^{-1}. A form factor χ is used to account for the fact that the Voigt line profile overestimates the absorption of the far wings (Tran et al., 2011), especially at high pressure, essentially due to collision-induced intensity transfer between transitions (line-mixing effects) and to the finite duration of intermolecular collisions. Referring again to Haus et al. (2013), χ is set to 1 for each gas except CO_2. For CO_2 the form factor suggested by Tonkov et al. (1996) is used from 2000 cm^{-1} to 7500 cm^{-1} and that by Bézard et al. (2009) from 7500 cm^{-1} to 10000 cm^{-1}. The two parametrizations are given in Table 1. Table 2 summarises all the parameters used for the absorption coefficients computation.

The CO_2 *continuum* absorption is also accounted for (Haus and Arnold,

Table 1: Parametrizations of the χ factor depending on distance from the line centre ν_0. In the Table, $|\Delta\nu| = |\nu - \nu_0|$

Tonkov et al. (1996)		Bézard et al. (2009)	
$\|\Delta\nu\|$ (cm^{-1})	χ	$\|\Delta\nu\|$ (cm^{-1})	χ
$\|\Delta\nu\| < 3$	1	$\|\Delta\nu\| < 3$	1
$3 < \|\Delta\nu\| < 150$	$1.084^{(-0.027\|\Delta\nu\|)}$	$3 < \|\Delta\nu\| < 60$	$1.051^{(-\|\Delta\nu\|/60)}$
$150 < \|\Delta\nu\| < 300$	$0.208^{(-0.016\|\Delta\nu\|)}$	$\|\Delta\nu\| > 60$	$0.6671^{(-\|\Delta\nu\|/110)}$
$\|\Delta\nu\| > 300$	$0.025^{(-0.009\|\Delta\nu\|)}$		

Table 2: Overview of the parametrizations used to compute gases absorption properties.

Gas	Spectral band cm^{-1}	Database	Intensity threshold cm^{-1}/(molecule cm^{-2})	Cut-off cm^{-1}	χ
CO_2	2000-7500	HOTBASE	10^{-35}	125	Tonkov et al. (1996)
	7500-10000	HOTBASE	10^{-35}	250	Bézard et al. (2009)
H_2O, CO	2000-10000	HITEMP	10^{-28}	125	1
SO_2, OCS, HCl, HF	2000-10000	HITRAN	10^{-28}	125	1

Table 3: CO_2 continuum parameters for spectral bands.

Band centre (cm^{-1})	9804	9091	8475	7813	7634	5747	4348	2326
Band centre (µm)	1.02	1.10	1.18	1.28	1.31	1.74	2.30	4.30
Continuum (cm^{-1} $amagat^{-2}$ x 10^{-9})	0.025	0.45	0.15	0.76	-0.59	4.1	43	0

1 amagat = 2.686777 x 10^{19} molecules cm^{-3} at T=0°C and p=1 atm

2010; Tran et al., 2011; Haus et al., 2013). It is worth to remember that the definition of the continuum is empirical and it is used as a correction term in the simulations. Thus, the continuum is always related to the definition of the spectroscopic quantities (e.g. the line intensities) and the parameters simulations (e.g. the line cut-off). For consistency, the continuum defined by Haus et al. (2013) is considered. Its dependency on the spectral interval is reported in Table 3. Other species than CO_2 should account for similar continuum parametrizations but, due to their low abundance on the Venus' atmosphere, their continuum absorption is neglected.

The overall contribution of single gas is evaluated through its total optical depth X, integrated from TOA to the ground. In Figure 4 it is shown that CO_2 dominates the absorption in almost the whole spectrum, with the exception of some limited bands. The altitude where the total weighting function reaches the maximum value is computed for the gas component (not shown here). It is noticed that at VIRTIS shortest wavelengths the gases of the Venus' atmosphere present some strong atmospheric windows at 1.0 µm, 1.1 µm and 1.18 µm while very absorptive gas bands are located at 2.7 µm ($\nu_1 + \nu_3$ band of CO_2) and 4.3 µm (ν_3 band of CO_2).

The coefficients for molecular Rayleigh scattering are computed as sug-

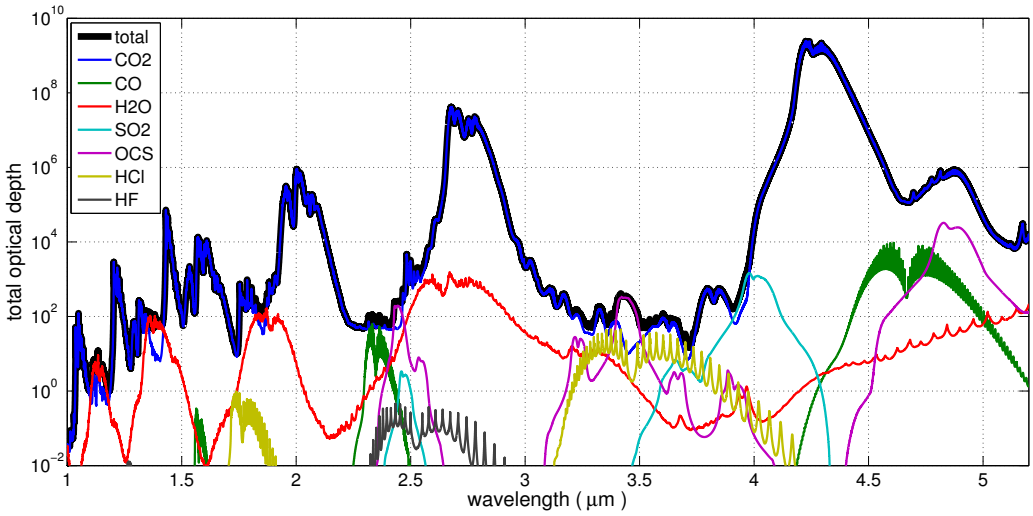

Figure 4: Total optical depth, from TOA (100 km altitude) to the ground, for single gas species, computed for the VIRA 45 profile.

gested by Maiorov et al. (2005) only for the two most abundant species: CO_2 and N_2. The contribution of minor constituents is negligible, as well as the dependence of the refractive index on temperature and pressure. Dependence of the scattering coefficient on $1/\lambda^4$ makes the Rayleigh scattering very important at around 1 µm, secondary at 1.5 µm and completely negligible for wavelengths larger than 2 µm.

4.2. Clouds and hazes

Aerosols optical properties are computed based on Mie scattering theory using the Scattnlay code by Peña and Pal (2009). The chemical composition of the Venus' aerosols is supposed to be an aqueous solution of sulphuric acid with varying concentration, by weight, between 75% and 98% (Mills et al., 2007). It is believed that H_2SO_4 formation mainly occurs by photochemical processes at about 62 km altitude from H_2O and SO_2 of volcanic origin.

The main cloud deck on Venus extends all over the planet between about 48 and 70 km of altitude (Knollenberg and Hunten, 1980). The cloud top level is usually defined as the height where the aerosols optical depth, integrated from TOA at 1 µm, becomes unity (Esposito et al., 1983; Zasova et al., 2007). The vertical structure of the clouds is characterized by growth of aerosols size with decreasing altitude, so that the clouds can be divided into upper clouds (roughly, 60-70 km altitude), middle clouds (50-60 km) and lower clouds (48-50 km). The upper cloud layer shows a bimodal particle size distribution that contains relatively small particles and the number density increases with decreasing altitude. In the middle cloud layer the particle number density sharply decreases but the extinction coefficient and the mass load increase due to the presence of a third large kind of particles that turns the size distribution into a trimodal. In the lowest cloud layer the particle number density rises again to values similar to the uppermost layer, whereas mass load and extinction coefficient grow even more due to the great increase of large mode particles. Above the three cloud layers, sub-micrometer aerosols were observed, usually called hazes. Hazes in the upper atmosphere of Venus form in part by condensation of H_2SO_4 on meteoritic dusts (Kalashnikova et al., 2000; Gao et al., 2014) and in part they are the result of transport of small aerosols from the upper clouds layer. It is common use to define 3 (or 4) particles size distribution (PSD) types depending mainly on the size as deduced from Pioneer missions data (Kawabata et al., 1980; Knollenberg and Hunten, 1980). The PSDs are called *modes* (Figure 5).

– *Mode 1* is formed of small size particles, with typical modal radius equal to 0.3 µm. It is assumed that mode 1 is distributed throughout the whole

Table 4: Parameters used for the Reference log-normal distribution of cloud particles.

Mode	1	2	2'	3
r_m (µm)	0.3	1.0	1.4	3.65
σ	1.56	1.29	1.23	1.28

cloud layer and partially characterizes the upper hazes.

– *Mode 2* has modal radius equal to 1.0 µm and is mainly observed in the uppermost and middle layer of the cloud deck. It's the most studied and well-known.

– *Mode 2'* is also accounted for as a variation of mode 2 extending in the middle and low clouds. It is defined to describe the growth of mode 2 size with decreasing altitude and has modal radius equal to 1.4 µm.

– *Mode 3* represents the largest particles, with modal radius assumed to be 3.65 µm. It is present in the middle and lowermost layers of the clouds. Characterization of mode 3 is still unresolved (Mills et al., 2007; Zasova et al., 2007). Some observations of the Pioneer missions seem to be compatible with solid, non spherical, asymmetric, possible crystalline particles with irregular shape and chemical composition that may actually be different from the other modes (Knollenberg and Hunten, 1980) but no proposed solutions come to a definitive agreement up to now. In this work, mode 3 particles are considered as spherical particles made of H_2SO_4 in aqueous solution as well as the other modes, as usually considered in literature (Pollack et al., 1993; Tsang et al., 2008; Haus and Arnold, 2010; Haus et al., 2013).

One of the most commonly used parametrization in literature to describe

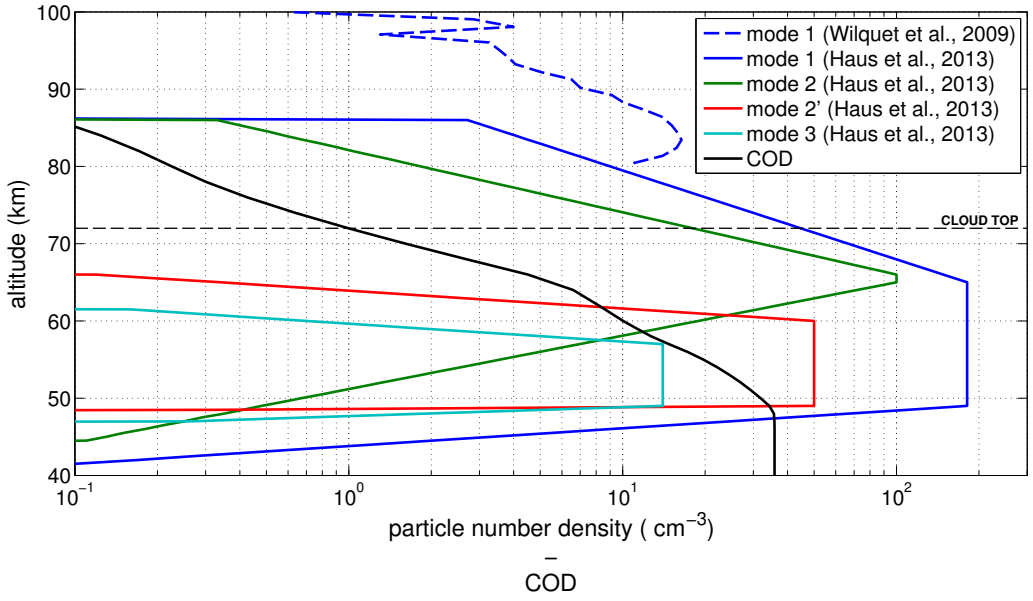

Figure 5: Particle number density as function of altitude for the four modes defined in the model. Cumulative optical depth (COD) from TOA at 1 µm is also reported in black. Cloud top is defined where COD=1.

Table 5: Parameters for the analytical description of the standard cloud model.

Mode	1	2	2'	3
z_b – Base altitude (km)	49	65	49	49
z_c – Layer thickness of constant particle number (km)	16	1	11	8
H_{up} – Upper scale height (km)	5	3.5	1	1
H_{lo} – Lower scale height (km)	1	3	0.1	0.5
N_0 – Particle number density at z_b (cm^{-3})	181	100	50	14

the Venus' aerosols is the one proposed by Pollack et al. (1993). It assumes that the modes are defined by log-normal particle size distributions, whose typical parameters are given in Table 4. As reference for this study, we assume a standard Venus model based on the parametrization suggested by Haus et al. (2013). Other possible clouds models are reported in Barstow et al. (2012). The particle number density as a function of altitude is defined as:

$$N(z) = \begin{cases} N_0(z_b)e^{-(z-(z_b+z_c))/H_{up}} & z > (z_b + z_c) \\ N_0(z_b) & (z_b + z_c) \leq z \leq z_b \\ N_0(z_b)e^{-(z_b-z)/H_{lo}} & z < z_b \end{cases} \qquad [cm^{-3}]$$

where the parameters are defined in Table 5. Usually, particle density distributions reported in literature don't consider aerosols above 86 km altitude. The analysis by Wilquet et al. (2009) of solar occultation observations by SPICAV, on board Venus Express, shows hazes well above this limit, up to 100 km. Therefore, the profile suggested by Haus et al. (2013) is completed with the results of Wilquet et al. (2009) (Figure 5). Some sensitivity studies

regarding the simulated upward spectral radiance with or without the presence of upper haze in the model have been performed. Results provide a radiance variation in the model ranging from 0.2% to 1.5%. This amount is at least one order of magnitude lower than that due to typical variations in the main cloud parameters. We thus assume that the contribution of the upper atmospheric hazes is secondary for the radiative transfer calculations. The nadir radiance field measured at TOA is mostly driven by processes occurring in layers below 80-85 km.

Common assumption for particles composition is a 75% or 84% solution by weight of H_2SO_4 for all the modes, along the whole vertical extent of the cloud layer. The 75% solution is the widest accepted value in literature (Pollack et al., 1993; Zasova et al., 2007; Grassi et al., 2008; Tsang et al., 2008; Bézard et al., 2011; Haus et al., 2014) and it will be the reference assumption in our Venus standard model. Nevertheless, some authors pose doubts on this assumption. In fact,**Krasnopolsky (2012, 2015)** states that the widespread value of 75% at the clouds top is incompatible with spectroscopic data and requires the H_2O mixing ratio of 25 ppm at 68 km that is not supported by the observations. Furthermore, other authors suggest that an increment in sulphuric acid concentration could be possible when descending through the clouds as deduced by probes data (Knollenberg and Hunten, 1980; James et al., 1997; Mills et al., 2007) and microphysical modelling (Imamura and Hashimoto, 2001). To account for all these possible configurations of the H_2SO_4 solution we assume either that all the cloud layers have the same sulphuric acid concentration (75%, 84% and 96% in solution) or that a variable concentration along the vertical is present. In this latter case the

cloud deck is split in two parts depending on the particles size: modes 1 and 2 are dealt together as well as modes 2' and 3 . In particular it is assumed that modes 1 and 2 are representative of the upper clouds and modes 2' and 3 of the lower clouds. Sulphuric acid mixtures of 75%/84%, 75%/96% and 84%/96% are tested, with the first term (referred to the upper part of the clouds) always lower than the second one (referred to the lower cloud). The refractive indexes used are those described in Palmer and Williams (1975)

4.3. The reference radiance spectrum

The software package libRadtran (Mayer and Kylling, 2005) is used to create a database of synthetic spectra to be compared with VIRTIS observations. A discrete ordinate method code (DISORT) developed by Stamnes et al. (1988, 2000) performs calculations in a plane-parallel atmosphere. The latest implemented version CDISORT by Buras et al. (2011) is used in this work. The output of the solver, convolved with the VIRTIS Instrumental Line Shape (ILS), is a synthetic spectrum observed at nadir (100 km altitude, TOA), to be compared with an observed VIRTIS spectrum. The spectrum shown in Figure 6 is obtained with the most common parametrizations for the Venus' clouds: atmospheric profile VIRA 45, particles of sulphuric acid in 75% solution, modal radii of the cloud modes 1, 2, 2' and 3: r_1=0.3 µm, r_2=1.0 µm, $r_{2'}$=1.4 µm, r_3=3.65 µm. The mode scale factors are assumed $f_1=f_2=f_{2',3}=1$ (see section 5.4). Since all the basic cloud parameters are assumed to correspond to the standard values found in literature, such a spectrum will be referred in the following text as the *reference model* and indicated with R_{ref}.

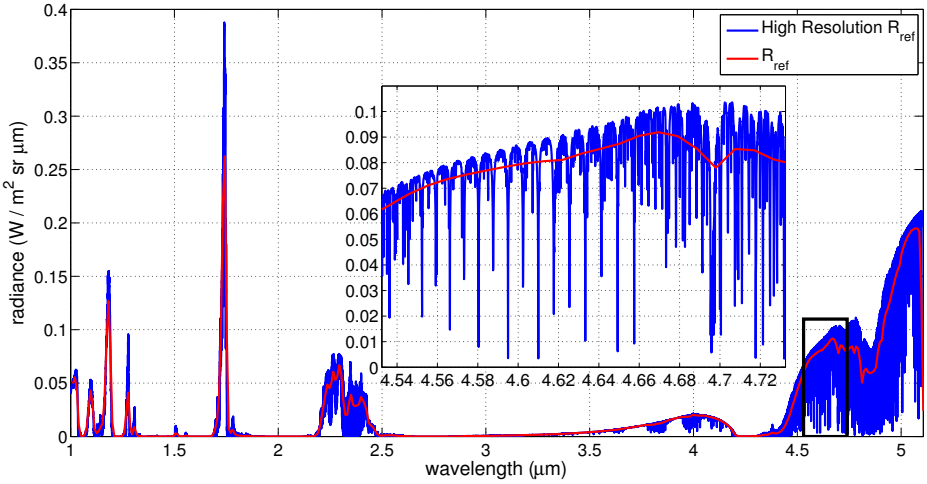

Figure 6: Reference model spectrum R_{ref}: 75% H_2SO_4, VIRA 45, r_1=0.3 µm, r_2=1.0 µm, $r_{2'}$=1.4 µm, r_3=3.65 µm, f_1=f_2=$f_{2',3}$=1. Blue line: libRadtran output with wavelength grid step of 0.1 nm. Red line: convolution of the high resolution output with the VIRTIS ILS. The inset plot zooms out the selected black rectangle.

5. Sensitivity analysis

Some radiance sensitivity studies are performed for different simulation parameters. The present analysis was useful to identify which parameters should be varied for the definition of the synthetic radiance dataset and their range of variation. The spectral bands used for the retrieval are also here identified.

5.1. Gases and aerosols

First, the bulk effect of gases and aerosols (clouds and hazes) is evaluated separately. Radiative transfer in the atmosphere is simulated assuming only one of the two components exists (Figure 7). Simulated brightness temperatures show the main role of the gaseous component corresponding to CO_2 absorption maxima at 2.0, 2.7 and 4.3 µm. Aerosols effects (the reference model is assumed) dominate between 3 and 5 µm, with the exception of the ν_3 band of CO_2, where radiation mainly comes from layers above the cloud top, from about 67 to 90 km. At other wavelengths, contributions of the two components have similar impact. In particular, in the atmospheric windows at 1.74 and 2.3 µm, as well as at shorter wavelengths, the reference spectrum shows that a significant amount of radiance comes from the lowest part of the atmosphere.

5.2. Surface albedo

At the VIRTIS shortest wavelengths, the radiance observed at TOA depends on the atmospheric characteristics but it is also affected by the direct contribution of the Planet's surface. Previous studies report of a spectrally

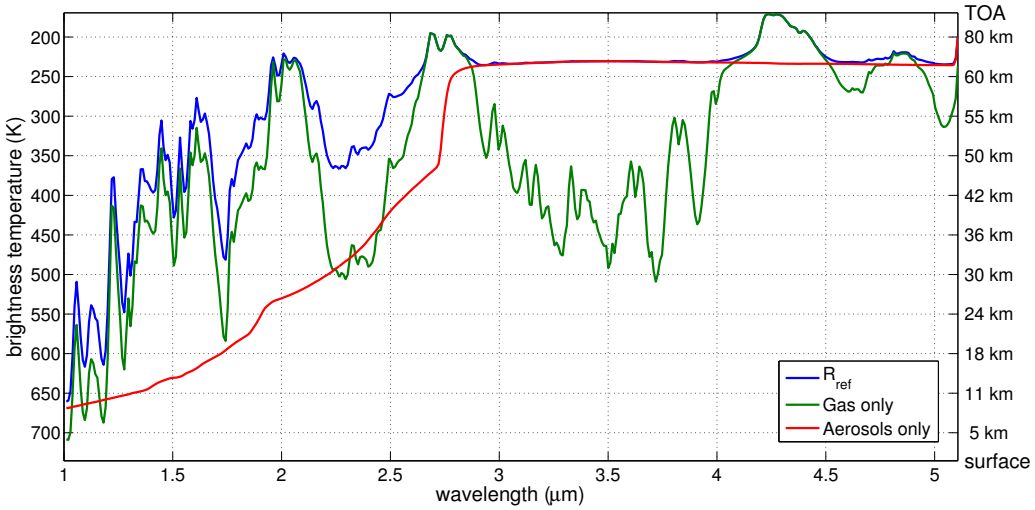

Figure 7: Simulated brightness temperature for a standard Venus' atmosphere and for hypothetical cases without aerosols or gas respectively (see legend). Tick marks on the right axis are altitude levels of the VIRA 45 profile obtained from temperature-height conversion.

constant Lambertian surface with the albedo assumed to be in the range 0.15-0.4 (Devaux and Herman, 1975; Hashimoto and Sugita, 2003; Arnold et al., 2008; Haus and Arnold, 2010). Simulations performed using the literature values show that some radiance sensitivity to surface albedo variation is observed only between 1.0 and 1.2 µm, with spectral radiance changes ranging from 2% to 8% in terms of radiance units. Since the albedo has a limited effect on radiance when compared to changes related with aerosols properties and cloud geometry (section 5.4) the synthetic database is computed assuming a constant albedo $a = 0.2$.

5.3. Sulphuric acid concentration

The H_2SO_4–H_2O solution concentration affects the optical properties of the aerosol's layers at different extent depending on the wavelength considered. Solutions with concentration of 25%, 38%, 50% are tested but they don't produce any spectral features in the 2.3 µm window, as is the case observed in the VIRTIS data. The featureless spectra for these assumptions is due to the large percentage of water in the solution that absorbs the upwelling radiance. Since these low concentration values do not allow any fit with the observed data they are not considered in our simulated dataset. Solutions with uniform concentration along the vertical clouds extent of 84% and 96% are compared to the reference case, that assumes a 75% concentration, as well to the non-uniform cases 75%/84%, 75%/96% and 84%/96%, with the two terms referring to the upper and the lower clouds respectively. Results (Figure 8) show limited differences at the VIRTIS shortest wavelengths and at 4 µm, whereas at 2.3 µm and for wavelengths larger than 4.5 µm differences are the largest. The radiance differences in these last two spectral interval

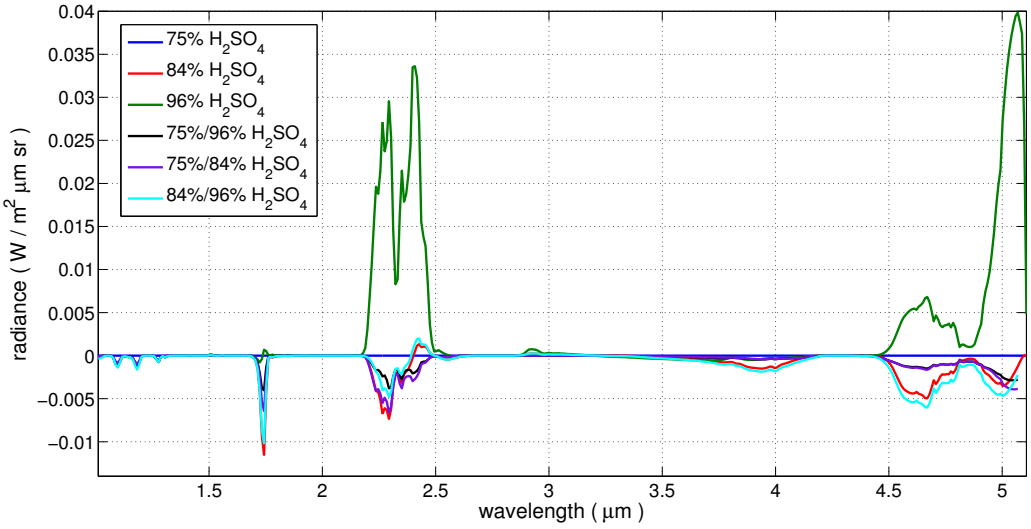

Figure 8: Radiance differences (R_{sim} – R_{ref}) for H_2SO_4 concentration solution variations. R_{ref}: 75% H_2SO_4.

are of the order of 12-75% of the signal. Each one of the selected concentrations shows peculiar features along the VIRTIS simulated spectrum and thus allowing a retrieval of the H_2SO_4–H_2O solution concentration. The uniform 96% case is the one with largest differences with respect to the reference case.

5.4. Particle number density and size distribution

Variations of the particle number density affects the simulated VIRTIS spectra at every wavelength with different intensity depending on the mode considered (Figure 9). Sensitivity studies with respect to the reference model are performed introducing a multiplicative factor f_i, where i refers to different aerosol modes. This parameter scales the particle number density equally at each altitude. Changes in the particle number density of the order of 0.1, 0.2, 0.5, 2, 5 and 10 are applied. Variations on the number concentration of

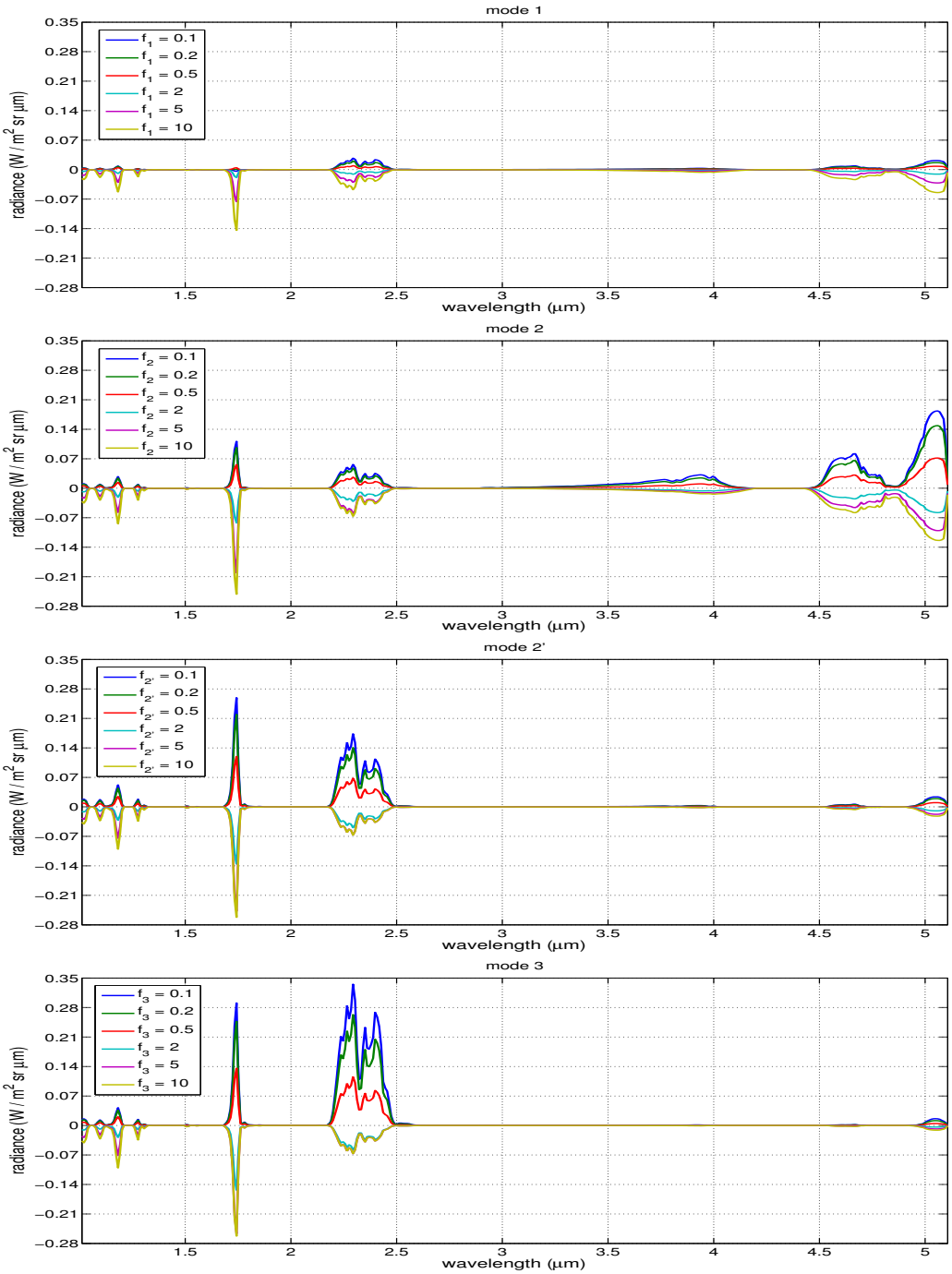

Figure 9: Radiance differences (R_{sim} – R_{ref}) for mode scale factor variations for the four modes. R_{ref}: f_i=1.

mode 1 show the least radiance sensitivity with respect to all other modes. Nevertheless, the upwelling radiance percentage variation is of the order of some percent when compared to the reference model. The most affected spectral intervals are shown in the upper panel of Figure 9. The largest effect is for radiance at around 1.7, 2.3 and beyond 4.5 µm. Note that most of the radiance at the longest VIRTIS wavelengths comes from the upper atmospheric layers (higher than 50 km) where only modes 1 and 2 have a not negligible particles concentration. Large sensitivity of upwelling radiances due to variation of f_2 is observed also for wavelengths larger than 3 µm. This characteristic does not occur for the cases accounting for modes 2' and 3 that, in turn, largely influence the radiance spectral features at wavelengths shorter than 2.3 µm, where upwelling photons mainly originates from the lower part of the atmosphere. The effect is particularly evident when reducing their number density, whereas a large mode scale factor (5 or 10) acts in a similar way for modes 2, 2' and 3. Since modes 2' and 3 show a very similar spectral behaviour for a number concentration variation and since they both describe the lower part of the cloud, their factor will be scaled together ($f_{2'}=f_3=f_{2',3}$) in the definition of the synthetic dataset.

Also variations in the modal radius r_i of the four modes are considered. Studies found in recent literature describe the aerosol microphysical properties using the modal radii defined by Pollack et al. (1993). Figure 10 shows the result of sensitivity tests concerning the modal radius of mode 2, showing a large sensitivity of the upwelling radiance to this parameter in all the observed windows. For the present study, realistic variations of the modal radius for the log-normal particle size distribution of each mode are assumed

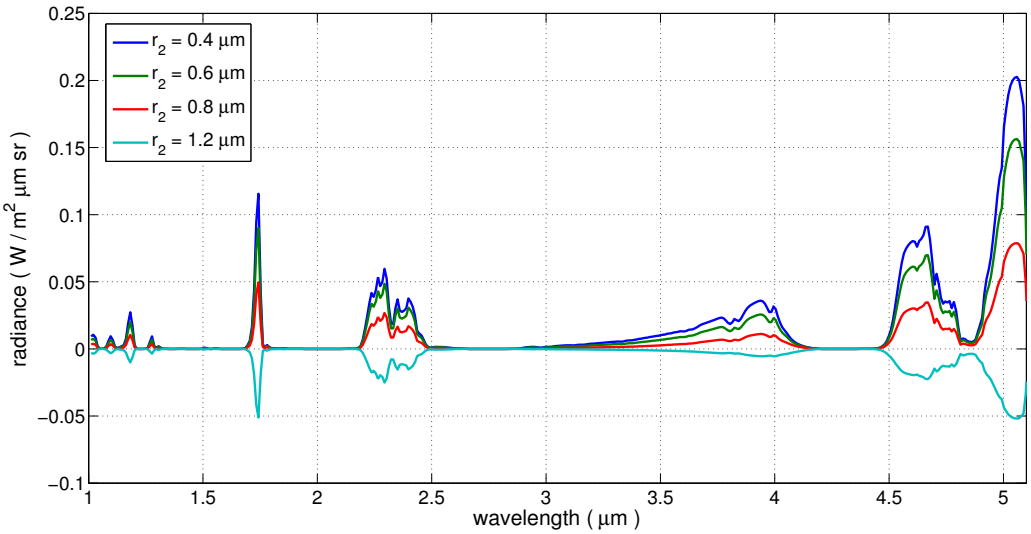

Figure 10: Radiance differences (R_{sim} – R_{ref}) for mode 2 radius variations. R_{ref}: r_2=1.0 µm

(Table 6). The parameter sigma of the distributions are kept fixed. Note that increasing the modal radius of mode 2, for example, acts in a similar way to the increase of the mode 2' scale factor, since the two modes become more similar. For these two modes, the two modal radii are varied but never allowed to assume the same value. Moreover, they are partially defined at different altitudes.

5.5. Temperature and pressure profiles

Since analysed VIRTIS spectra are observed in the latitude band between 25°N and 55°N, only two VIRA profiles are considered: VIRA 30 and VIRA 45. The maximum difference between the two profiles is about 3.7% in temperature at 59 km and 7.2% in pressure at 72 km. The influence on the retrieved spectrum is evident only for wavelengths above 3 µm. At the

VIRTIS shortest wavelengths most of the radiance comes from the lowest atmospheric layers where VIRA profiles are identical. Variation of radiance at 4 µm, due to change in VIRA profiles, is about 50% of that obtained with a mode 2 scale factor equal to 0.5 and reaches about 60% above 4.5 µm.

5.6. Summary of sensitivity tests

The upper panel of Figure 11 compares the effect on the simulated radiance of some parameters variations. A direct comparison among different parameters sensitivities is shown as an example of their quantitative effect on the radiance spectrum. The same panel of the **figure** also reports, for each window band, a list of the cloud, atmospheric or surface parameters most affecting the simulated radiances. The lower panel of Figure 11 highlights the **nonlinear** effect of the parameters on the spectral radiance. The plot shows the spectral variation of two kind**s** of residuals: in the first case the curve is obtained by summing the single solutions (three residuals in the example) obtained by changing one parameter at a time with respect to the reference model, whereas in the second case the residual is obtained by comparing the reference model to a simulated spectrum computed by assuming that all the three parameters are varied simultaneously from their reference values. The differences in the two plots are sensible and at some wavelengths larger than the average noise equivalent spectral radiance of the sensor in that spectral interval (see Section 7).

6. Synthetic dataset

An extensive dataset of synthetic spectra is created by assuming multiple atmospheric and clouds conditions. In addition to the aerosol particles

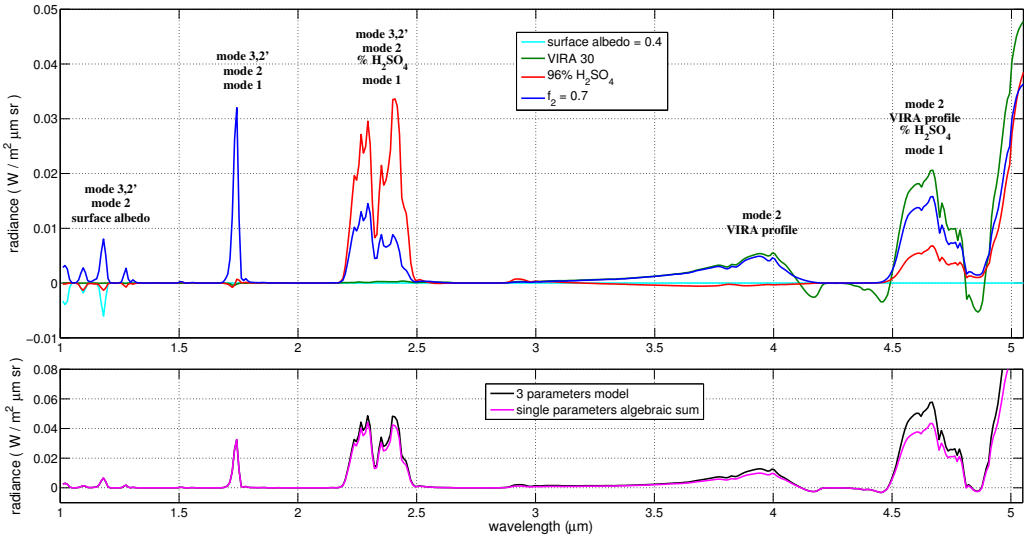

Figure 11: Top: Comparison between radiance differences (R_{sim} – R_{ref}) obtained as a response to single parameter changes with respect to their reference values. The modified parameters and their values are indicated in legend. The values of the reference model, R_{ref}, are: surface albedo=0.2, VIRA 45, 75% H_2SO_4, f_2=1. Main parameters affecting the simulated radiance at various spectral intervals are also listed and ordered in magnitude from top to bottom. Bottom: Radiance differences (R_{sim} – R_{ref}) obtained for the algebraic sum of the three models showed in the top panel (albedo excluded) and for a single simulation in which all the three parameters are changed simultaneously.

number density and the clouds height, usually considered in literature as free parameters, possible variations in the particles size distribution and in the sulphuric acid concentration within the cloud deck are assumed, usually considered as constants. To create the dataset, we first assume, for each of the considered parameters, the limits of variations (maximum and minimum values of the parameter). Then, we define the adequate step of variation within the maximum and minimum value. The parameters accounted for in the computations, their range limit and their step are shown in Table 6 (details about the parameters at Section 5). Since the number of possible parameters combinations is of the order of several billions it is impossible to simulate them all. **The step sizes of the parameters variation have been defined in accordance with the sensitivity analysis. An increse of the step sizes, in order to reduce the number of simulations, would mean to neglect important spectral features of the simulated radiance fields and would thus limit our analysis (see Section 5). Therefore, we rely on a subset of combination of the parameters' variation capable to adequately represent the variability of the entire system. To accomplish this task** we associate a sequential number to each parameters combination and select the simulations to be performed **by means of** pseudo-random values, obtained from the standard uniform distribution by a commercial numerical code (*rand* function in MATLAB®). Moreover, additional combinations are chosen in order to perform simulations of the basic cases frequently reported in literature. A final database with 10 227 different spectra is created, representative of the whole variety of the analysed VIRTIS spectra. Figure 12 shows that, within the three latitude bands considered,

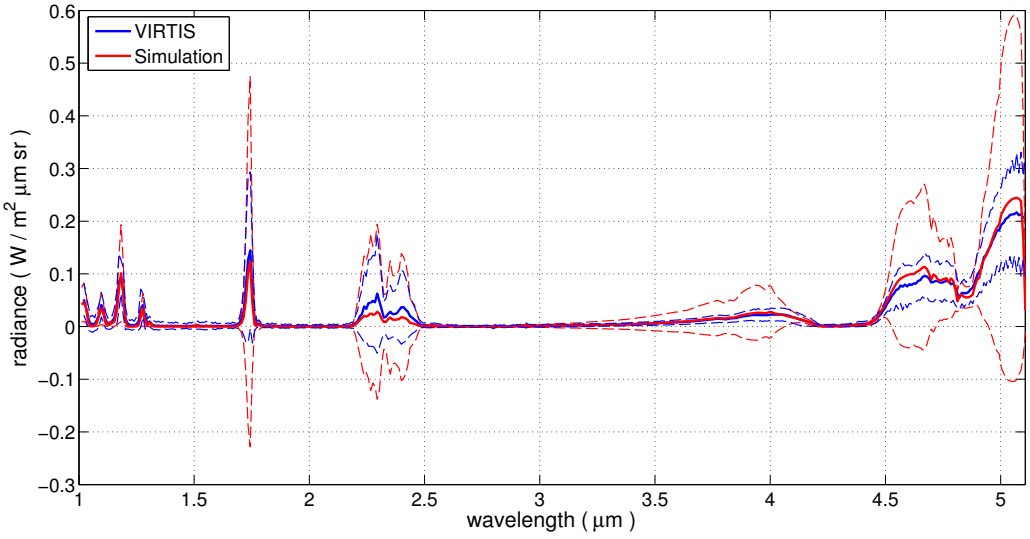

Figure 12: Mean spectrum obtained from all the VIRTIS nadir nocturnal observation (37635) between 35°N and 45°N (blue solid line) compared to the mean of all the simulated spectra (10227) obtained with libRadtran (red solid line). Broken lines are three standard deviations from the mean.

the mean spectrum of the sampled VIRTIS observations (plotted with three standard deviations) is consistent with the mean spectrum obtained from the simulated spectra (also plotted with three standard deviations). Some exceptions are encountered for very low values of the radiance, mostly due to the fact that LibRadtran always returns radiances with physical meaning (greater than zero) whereas some VIRTIS data show negative values because of fluctuations on the dark current, causing calibration errors (Erard, 2012).

7. Fitting methodology

The atmospheric and cloud parameters (model) are retrieved for each bin of observations. The retrieval methodology is based on the direct compari-

Table 6: Parameters of the model and their range of variation

Variable		Range or Values
p - T vertical profile		VIRA 30 - VIRA 45
H_2SO_4 concentration		75% - 84% - 96% 75%/84% - 75%/96% - 84%/96% [(1)]
Mode scale factor		
	f_1	0.1 to 2.0 (step 0.1)
	f_2	0.2 to 2.0 (step 0.1)
	$f_{2',3}$	0.7 to 2.0 (step 0.1)
Modal radius		
	r_1	0.1 - 0.2 - 0.3 - 0.4 - 0.5
	r_2	0.4 - 0.6 - 0.8 - 1.0 - 1.2 - 1.4 [(2)]
	$r_{2'}$	1.4 - 1.6 - 1.8 - 2.0
	r_3	2.80 - 3.65 - 4.40

[(1)] The two values refer to modes 1-2 (uppermost cloud layers) and 2'-3 (lowermost cloud layers) respectively.

[(2)] The value 1.4 is only used when $f_{2'} \neq 1.4$ to preserve a distinction between the two modes.

son of the observed radiance with every simulation composing the synthetic model datasets. The selection of the most appropriate model (i.e. the most accurate simulation) is obtained through the definition of the parameter γ. The parameter is used to evaluate how accurately each synthetic spectrum is reproducing any observed scene. The γ is defined as:

$$\gamma_j = \sqrt{\frac{1}{N}\sum_{i=1}^{N}[(R_{sim,j}(\lambda_i) - R_{bin}(\lambda_i))^2\ W(\lambda_i)]}\ , \quad W(\lambda_i) = \frac{\sigma_{tot}(\lambda_i)}{\sum_{i=1}^{N}\sigma_{tot}(\lambda_i)}$$

where i is the wavelength dependency, N is the total number of wavelengths accounted for in the minimization process, $\mathrm{R_{bin}}$ is the observed radiance, $\mathrm{R_{sim,j}}$ is the j-th simulated spectrum, W is the weight associated to each wavelength. The weight W is defined as the standard deviation σ_{tot} of all the VIRTIS observations (note that it is not the one computed for the mean radiance in the bin) within each latitudinal band (25-35°N, 35-45°N, 45-55°N) in nocturnal nadir looking geometry at the i-th wavelength, divided by the sum over wavelengths. The minimization criterion is based on the following considerations. Channels with high CO_2 absorption are not considered in the fitting procedure because the radiance does not show any sensitivity to clouds parameters at these wavelengths. Wavelengths larger than 4.5 µm are also excluded because the detector often saturates at the larger wavelengths and most of the data are missing. This fitting procedure focuses on spectral radiances collected in windows channels sensible to cloud parameters and weights more the channels that show the largest radiance variations globally (meant as latitudinal bands). The considered channels account for most of the natural variability observed in the data. In fact, the excluded channels sums to 5-6% of the overall spectra variability only. The window channels

provide the following result:

$$\sum_{i=1}^{N} \frac{\sigma_{tot}(\lambda_i)}{\sum_j \sigma_{tot}(\lambda_j)} \approx 95\%$$

The retrieval is then performed comparing the mean data of the bin with all the simulations in the synthetic dataset. The best model is selected as the one for which the minimum value of γ is obtained among all the simulated spectra. The best γ is compared with the mean noise associated to VIRTIS observations that is used as an a-priori threshold (Figure 13). A noise equivalent spectral radiance (NESR) is evaluated for some typical cases depending on detector temperature end exposure time. The mean NESR extracted from the data cube for a 0.3 s exposure at different temperatures, which are typical conditions for nadir observations, is about 10^{-3} W/(m^2 µm sr). A best fit is accepted and accounted for in the statistical analysis of the results if $\gamma \leq$ NESR. Otherwise, the fit is not inserted in the final statistics and it is assumed that the synthetic database is not representative of the observation. This criterion is very conservative in terms of radiance residuals minimization and is meant to obtain the most robust results possible. Such a procedure reduces the number of bins that can be accurately described with the current synthetic database by only 5.8%. The spectra of these rejected bins were collected during only 13 days over the 90 days of the sample. Moreover, it is possible to group them in 4 main periods, two of them close to the beginning of the mission and two close to its end (Figure 13). The same days with rejected bins are observed, with few exceptions, in the three latitude bands. A possible explanation is linked to dynamical events in the Venus' atmosphere during those days, that might have modified the clouds structure

under observation and moved them out of the conditions accounted for in our database. This possibility requires to be further investigated with dynamical data but it is out of the purpose of this work and anyway affects only a small subset of our dataset. Nevertheless, an analysis of the results concerning the data excluded from the final discussion show very similar retrieved parameters distributions to those obtained in case of the accepted bins, described at Section 8.

The plot in Figure 13 also shows the performance of the fit in case the reference Venus' atmosphere is used and compared to bin data. It is demonstrated that the initial reference assumptions on clouds are not enough accurate in describing the observations since all the γ obtained from the R_{ref} are larger than the NESR, with the exception of a couple of cases in which they are anyway of the same order. Ratios between the γ parameters calculated for the best fit of each bin and the reference model reveal a gain, defined as $1 - \gamma_{bin}/\gamma_{ref}$, greater than 50% for the majority of the bins, with a maximum of 97.8%, and never below 26% when the discarded bins are not considered (they would have a minimum gain of 12.4% anyway), hence a sensible improvement in the clouds representation is obtained.

8. Analysis

The analysis of the results concerning the best fits, when applied to the entire VIRTIS dataset, is in contrast with the widespread assumed hypothesis that an homogeneous value of 75% H_2SO_4 solution is present in the whole cloud layer. As already said, this assumption is extensively used in literature (Pollack et al., 1993; Zasova et al., 2007; Grassi et al., 2008; Tsang et al.,

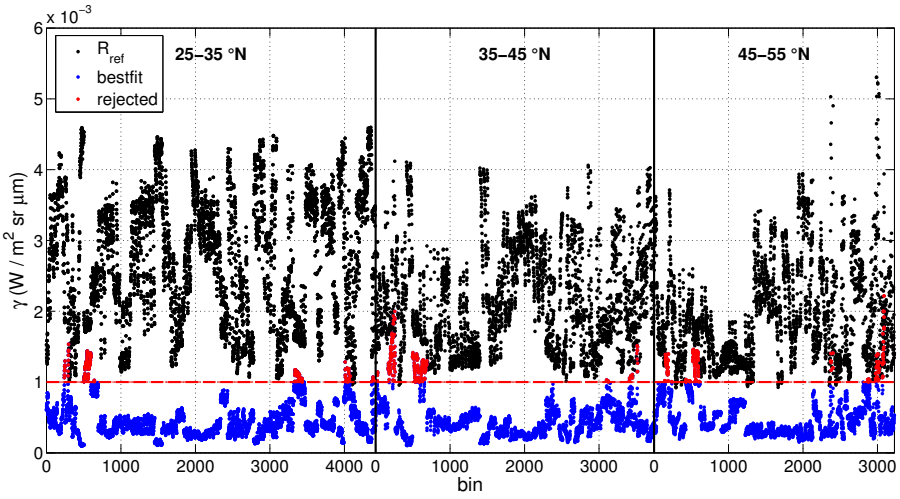

Figure 13: Root mean square γ calculated with the reference model (black dots) and the best fit model (blue dots) for the three latitude bands. Fits obtained with $\gamma \geq 10^{-3}$ are assumed not enough accurate and they are rejected (red dots). Each dot represents a bin, numbered with increasing order from the first to the last day of the VIRTIS observations.

2008; Bézard et al., 2011; Haus et al., 2014). Nevertheless, the results show that none of the bins is fitted by a synthetic spectrum with a 75% concentration (Figure 14). This consideration holds not only in the 75% case, but also for the homogeneous 84% case that has no correspondence with the observations except that for only two cases in the 35-45°N band (it is 0.06% of the total cases in that latitudinal band). The constant sulphuric acid concentration along the vertical extent does not allow an accurate fit of the simulation to the VIRTIS spectra. In particular, such assumption does not reproduce sufficiently well the observed radiance spectral peak at 1.74 µm and others radiance spectral features. In these windows intervals the data present large standard deviations and hence the weights of the fitting procedure are elevated. Assuming different H_2SO_4 concentrations in the cloud layers significantly improves the fit quality. In particular, the 1.74 µm window fit is improved and an excellent fit of the spectrum at every wavelength is obtained in most of the cases. An example of best fit spectrum is shown in Figure 15. The usual assumption of relatively low and vertically homogeneous concentration (75%) is then rejected by the present analysis. On the contrary, the hypothesis of a stratified cloud with higher acid concentration in the bottom layer, up to 96%, is strongly suggested. Note that among the vertically non-homogeneous concentration, the 75%/84% is present in only about 9% of the fits. This configuration has its maximum at 25-35°N and its minimum at 45-55°N. Pure 96% models represent only a little percentage of the retrieved sample but they are not negligible. Note that their number increases from lower to higher latitudes. The latter two cases suggest a poleward increase of the sulphuric acid concentration for the considered

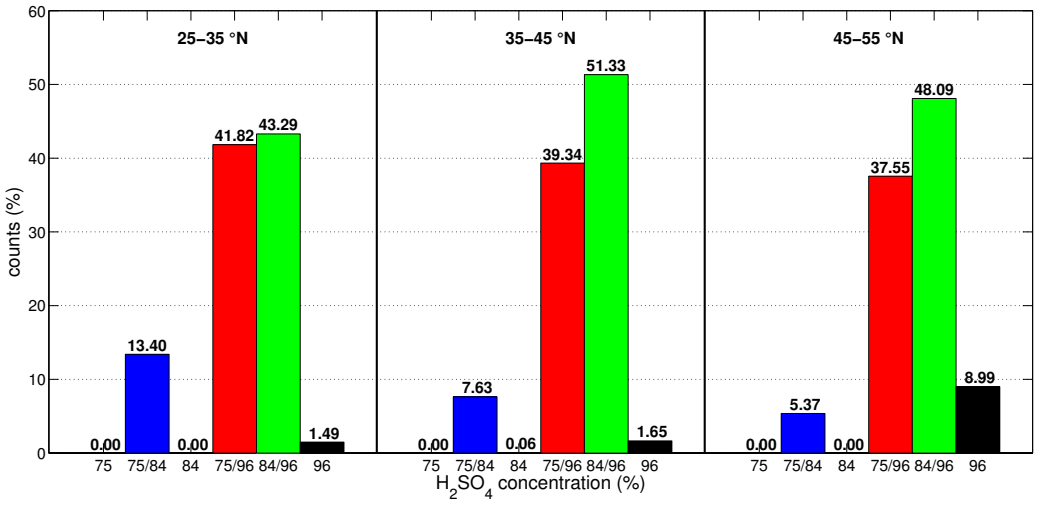

Figure 14: Percentage counts of the distribution of the retrieved sulphuric acid concentrations. Results are plotted for three latitudinal bands. Double values in the abscissa refer to the concentration of the upper and the lower cloud respectively.

latitudinal bands. The 75%/96% and 84%/96% are the most commonly retrieved models representing more than 85% of the cases for all the three latitudinal bands. Using the stratified concentration assumption allows to adequately fit also the short-wavelength side of the 4.3 µm band (Figure 16) which is known to present large residuals when the vertically uniform 75% concentration is assumed in the model (Grassi et al., 2014).

Figure 17, left column, shows the percentage occurrence of the retrieved aerosols modal radii for the four modes all over the considered dataset. Modes 2 and 2' have the best accordance with the reference model of Pollack et al. (1993). The peak values of the histograms are around 0.8-1.0 µm and 1.4 µm respectively for modes 2 and 2', to be compared with modal radii of 1.0 µm and 1.4 µm as assumed in the reference model. A weak latitudinal

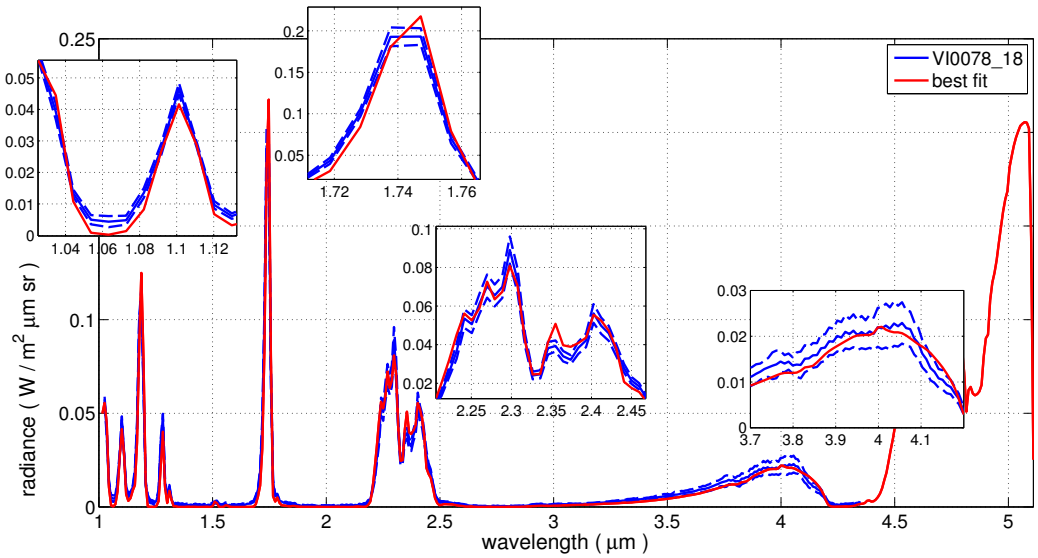

Figure 15: Best fitted simulation (red) against a VIRTIS bin obtained from 19 averaged spectra of the cube VI0078_18 (08/07/2006). Broken lines are plotted at three standard deviations from the mean. Bin edges: lon. 232.164–232.276°E, lat. 38.2039–38.3903°N. Best fit model: 75%/96% H_2SO_4, r_1=0.5 µm, r_2=0.8 µm, $r_{2'}$=1.8 µm, r_3=3.65 µm, f_1=0.2, f_2=1.8, $f_{2',3}$=0.8, VIRA 45.

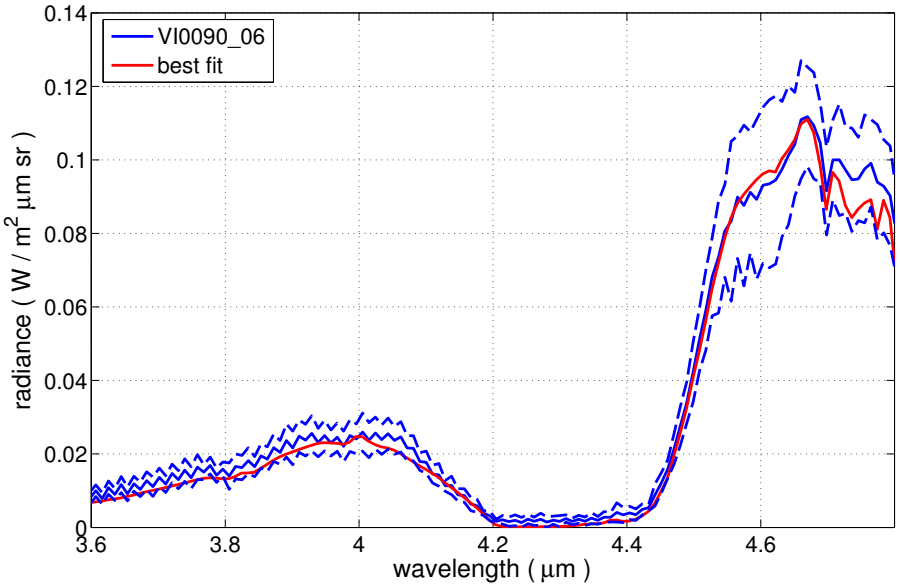

Figure 16: Best fit spectrum for 16 averaged spectra of the cube VI0090_06 (20/07/2006). Broken lines are plotted at three standard deviations from the mean. Bin edges: lon. 249.780–249.966°E, lat. 35.8163–35.9906°N. Best fit model: 75%/96% H_2SO_4, r_1=0.5 µm, r_2=0.6 µm, $r_{2'}$=1.4 µm, r_3=2.80 µm, f_1=1.4, f_2=2.0, $f_{2',3}$=1.0, VIRA 30.

trend is observed, suggesting an increase of the modal radius for mode 2 and a decrease for modal radius of mode 2' when moving from the southern to the northern belt. Mode 3, whose characteristics are still highly debated, has largest number of counts for the modal radius of 2.8 µm, hence for particles 55% smaller in volume than those assumed in the reference literature model (3.65 µm). Nevertheless, the reference modal radius fits the observations for a significant percentage of the retrieved cases that increases from south to north (up to more than 40%). Differences larger than expected in the retrieved modal radius are observed for mode 1. Most of the analysed VIR-TIS radiances are well fitted when the assumed radius r_1 is equal to 0.5 µm instead of the reference 0.3 µm. The reference value is encountered in less than 20% of the total cases. To note that mode 1 particle number density is largely reduced with respect to the standard. The most common retrieved mode scale factor is about 0.2 (Figure 17, right column) suggesting a less dense mode 1 particle concentration than supposed. Mode 2 scale factor is found to be quite variable all over the considered range. The most common values are 0.8 and 1, nevertheless their occurrence is never higher than 25%. Note that for each latitudinal band the factor 0.4 and 2.0 are observed in more than 10% of the cases each, thus suggesting considerable variations of the particle concentrations in the Venus' atmosphere between 60 and 70 km of altitude. Modes 2' and 3 are instead retrieved in larger number density than expected, with an averaged increase of about 30%. This is in accordance with what found by Haus et al. (2013) (who defined the initial cloud model adopted in section 4.2), who retrieved a mode 3 scale factor of 1.5-1.6.

The two considered atmospheric profiles, VIRA 30 and VIRA 45 are also

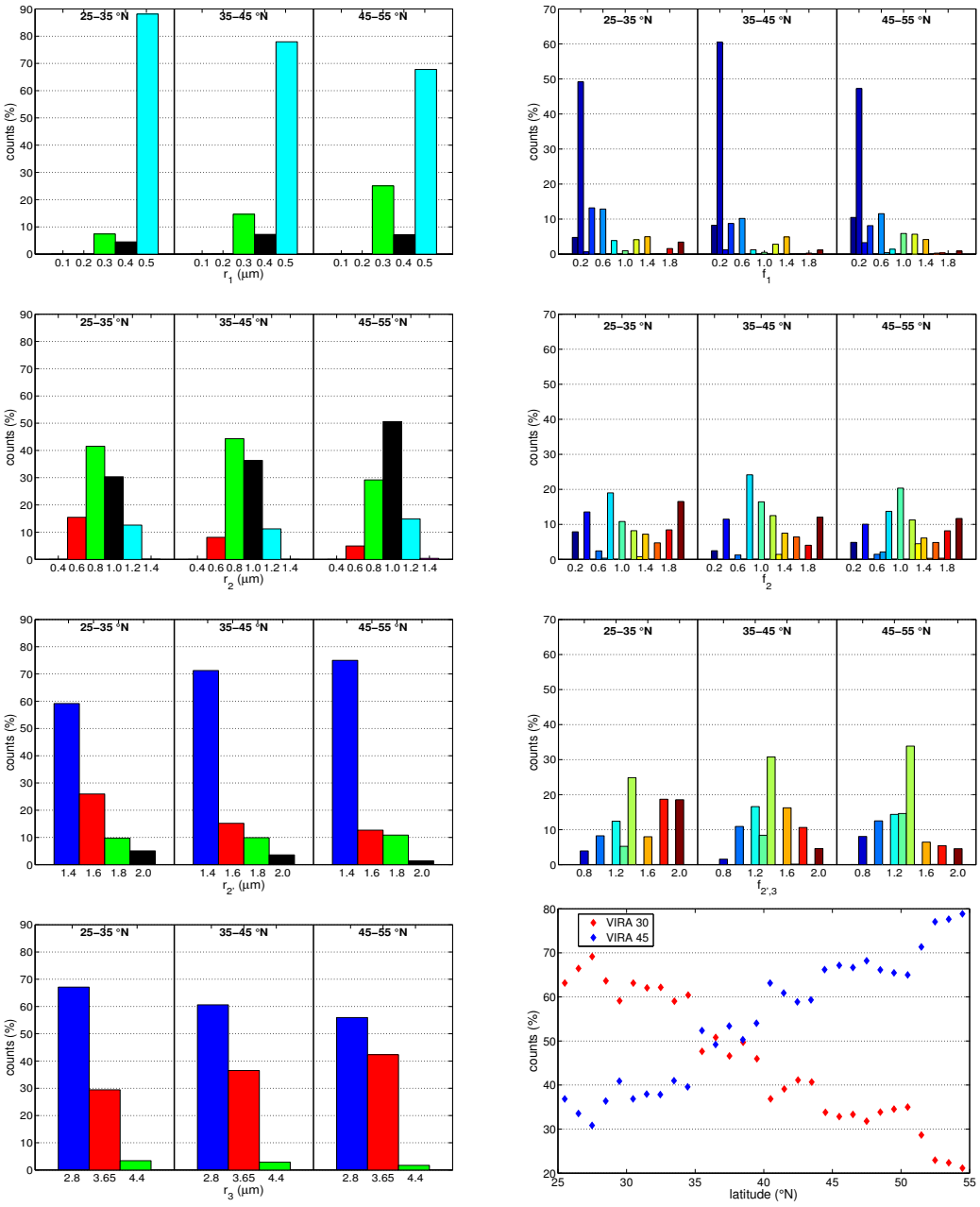

Figure 17: Left column: Occurrence of the retrieved values of modal radii r_i for selected latitudinal bands. Right column (three upper panels): Occurrence of the retrieved mode scale factors f_i. Bottom right: Occurrence of the retrieved atmospheric profile as a function of latitude.

varied in our synthetic dataset. The retrieval results are shown in Figure 17, bottom right panel. As expected, the majority of the best fits (more than 60%) are associated to VIRA 30 profile below 35°N and to VIRA 45 above 40°N.

Note that the uncertainties associated to each single estimated parameter are difficult to define since, as shown in Section 5.6, the combined effect of multiple parameters is **nonlinear**. We have evaluated the variation of the γ index for the firsts five best fit of each observation bin. It is found that γ decreases averagely of about 6% from the fifth to the first best fit. The improvement of the fitting with respect to the reference model is shown to be about 1 order of magnitude in most of the cases. The five best models fitting each bin, are also analysed to evaluate the robustness of the results in terms of stability of the retrieved parameters. In other words, we expect that the parameters that mostly affect the radiance spectrum are found to have the same value, or similar ones, for the five best fits. In Section 5 it is shown that over the whole spectrum, the modal radii show the largest radiance sensitivity among all the considered cloud parameters. Therefore, the standard deviation of modal radius is computed for the best five fits of each bin and it is found that it is averagely lower than the step size considered in the radius variation for each one of the four modes.

9. Summary and Conclusions

VIRTIS-M IR archive span a long time interval, about 5 years long. A statistical analysis has been performed on 65 orbits, containing nocturnal nadir observations in the latitude band between 25°N and 55°N. The obser-

vations have been averaged into bins of 0.2° x 0.2° of longitude x latitude and a forward model has been defined to retrieve atmospheric and clouds properties for each bin. This has required the provision of an extensive dataset of simulated synthetic spectra. The dataset creation has started from an initial reference model based on previous results found in the literature: vertical profiles of temperature and pressure are referred to the standard VIRA (Seiff et al., 1985), VMR profiles of gases are from Haus and Arnold (2010), clouds and hazes particle number density distributions are derived from the work of Haus et al. (2013) and Wilquet et al. (2009) respectively, clouds chemical composition and particle size distributions are referred to Pollack et al. (1993). This reference model has been modified in its parameters to obtain an extensive ensemble of models capable to describe the variability of the Venus' atmosphere. Synthetic radiances are computed using a multiple scattering line-by-line procedure. A *best fit* process has been implemented to establish the best model for each VIRTIS observation **over the the full spectrum from 1 to 4.5 µm, where radiance sensitivity to clouds' microphysics and chemistry is very large**. The mean difference between each VIRTIS spectrum and the synthetic one obtained with the reference model is always larger than the mean noise on VIRTIS data, suggesting that the reference literature model is ever inadequate to describe the Venus' atmosphere at the latitudes considered in the present study. **The differences in the retrieved cloud parameters with respect to the Venus standard model affect both the microphysical and the chemical properties that for the first time have been inferred together from remote sensing data.**

Particle size distributions representing the four modes of Venus clouds are varied in their modal radii with respect to accepted mean values. Our analysis suggests that the VIRTIS spectra are better fitted with an effective size of mode 1 particles around 0.5 µm. This view is consistent with previous findings of Wilquet et al. (2009): a second haze population, with substantial bigger particles (>0.5 µm) than the standard 0.3 µm mode needs to be added to fit the limb observations of SIPCAV/SOIR instrument. Similarly, in their analysis of Akatuski data, Satoh et al. (2015) found appropriate to introduce a small amount of mode 2' particles above the 75 km level (see their Table 4). The analysis of Shalygina et al. (2015) of VMC-derived phase functions suggests the existence of a substantial amount of particles with modal radius around 0.9 µm in the clouds and/or in the upper haze, especially evident at intermediate southern latitudes (40-60°S). Results from both Satoh et al. (2015) and Shalygina et al. (2015) are, at least qualitatively, compatible with our detection of relatively large particles (>0.3 µm) in the upper haze. The best fit process shows that modes 2 and 2' have the best accordance with the reference model in terms of particle size. The main retrieved values for their modal radii are 0.8/1.0 µm and 1.4 µm respectively, to be compared with 1.0 µm and 1.4 µm of the reference ones. The decrease of effective size of mode 2' particles with latitude inferred from our analysis is in accordance with findings of Shalygina et al. (2015). However, it shall be noted that these authors performed an analysis on solar radiation reflected at the top of the atmosphere and therefore a proper comparison shall probably be made with the upper mode 2, where an opposite behaviour is found. Results concerning mode 2 concentration show a very high variability of number density in the

Venus' atmosphere between 60 and 70 km of altitude. A lower variability is observed in the lower clouds for modes 2' and 3 but their particle number density is increased by about 30-40% with respect to the reference values in most of the cases, that is a similar to what found by Haus et al. (2013). More than half of the best fit models show mode 3 particles about 55% smaller in volume than the reference one, even though the size of 3.65 µm is largely present in the retrieval results. The increase of mode 3 particle size with latitude is qualitatively consistent with the increase of total opacity of deep clouds toward the pole reported by Cardesín Moinelo et al. (2008) from VIRTIS observations over the southern hemisphere and with the variations of deep cloud size invoked to justify the NIMS observations by Carlson et al. (1993) and Grinspoon et al. (1993).

The chemical composition of the clouds is usually considered in models as an aqueous solution of sulphuric acid at 75%, uniform along the whole vertical extent of the clouds layer. Nevertheless, many authors suggest that the acid concentration increases with decreasing altitude, up to 98% in the lower clouds. The synthetic dataset accounts for vertically uniform clouds with constant H_2SO_4 concentration with values 75%, 84% and 96%, and also for clouds with vertically variable concentration, separated into upper clouds (modes 1 and 2) and lower clouds (modes 2' and 3), with higher acid concentration in the lower layers. **For the first time, also the 75%/84%, 75%/96% and 84%/96% combinations have been tested in a retrieval scheme in conjunction with variation of the microphysics and density of the cloud particle size distribution.** None of the VIRTIS spectra are fitted by a synthetic spectrum realized with the usual 75%

hypothesis. Also the 84% case has no correspondence with the observations, except for only two cases, and only about 8% of the bins are fitted by a mixed cloud 75%/84%. On the contrary, the hypothesis of a stratified cloud with high acid concentration in the bottom layer, up to 96%, is strongly supported by about 92% of the retrievals. In particular, the 84%/96% combination results in more than half of the observations. Using the stratified cloud allows to adequately fit the observed radiance in the short-wavelength side of the 4.3 µm band which is known to be problematic when the 75% concentration is assumed in the model. Pure 96% models represent only a little percentage of the retrieved sample but they are not negligible and outnumber the frequency of occurrence of lower uniform concentrations. Our analysis suggests also a latitudinal increase of sulphuric acid concentration in the clouds moving from the equator toward the poles. This last finding confirms the previous study by Barstow et al. (2012) based on VIRTIS observations over the southern hemisphere.

References

References

Andreichikov, B.M., Akhmetshin, I.K., Korchuganov, B.N., Mukhin, L.M., Ogorodnikov, B.I., 1987. VEGA 1 and 2 X-ray radiometer analysis of the Venus cloud aerosol. Kosmicheskie Issledovaniia 25, 721–736.

Arnold, G., Haus, R., Kappel, D., Drossart, P., Piccioni, G., 2008. Venus surface data extraction from VIRTIS/Venus Express measurements: Estimation of a quantitative approach. J. Geophys. Res. Planets 113. doi:10.1029/2008JE003087.

Barstow, J., Tsang, C., Wilson, C., Irwin, P., Taylor, F., McGouldrick, K., Drossart, P., Piccioni, G., Tellmann, S., 2012. Models of the global cloud structure on Venus derived from Venus Express observations. Icarus 217, 542–560. doi:10.1016/j.icarus.2011.05.018.

de Bergh, C., Moroz, V., Taylor, F., Crisp, D., Bézard, B., Zasova, L., 2006. The composition of the atmosphere of Venus below 100 km altitude: An overview. Planet. Space Sci. 54, 1389–1397. doi:10.1016/j.pss.2006.04.020.

Bézard, B., Fedorova, A., Bertaux, J.L., Rodin, A., Korablev, O., 2011. The 1.10- and 1.18-μm nightside windows of Venus observed by SPICAV-IR aboard Venus Express. Icarus 216, 173–183. doi:10.1016/j.icarus.2011.08.025.

Bézard, B., Tsang, C.C.C., Carlson, R.W., Piccioni, G., Marcq, E., Drossart, P., 2009. Water vapor abundance near the surface of Venus from Venus Express/VIRTIS observations. J. Geophys. Res. Planets 114. doi:10.1029/2008JE003251.

Buras, R., Dowling, T., Emde, C., 2011. New secondary-scattering correction in DISORT with increased efficiency for forward scattering. J. Quant. Spectrosc. Radiat. Transfer 112, 2028–2034. doi:10.1016/j.jqsrt.2011.03.019.

Cardesín Moinelo, A., Piccioni, G., Migliorini, A., Drossart, P., 2008. Global Mapping of Venus' Atmosphere Using Accumulated Projections of Virtis Venus Express Observations. AGU Fall Meeting Abstracts .

Carlson, R.W., Kamp, L.W., Baines, K.H., Pollack, J.B., Grinspoon, D.H., Encrenaz, T., Drossart, P., Taylor, F.W., 1993. Variations in Venus cloud particle properties: A new view of Venus's cloud morphology as observed by Galileo Near-Infrared Mapping Spectrometer. Planet. Space Sci. 41, 477–485. doi:10.1016/0032-0633(93)90030-6.

Devaux, C., Herman, M., 1975. Venus: Cloud optical depth and surface albedo from Venera 8. Icarus 24, 19–27. doi:10.1016/0019-1035(75)90154-2.

Erard, S., 2012. VenusExpress-VIRTIS: To Planetary Science Archive Interface Control Document (EAICD). European Space Agency, Research and Science Support Department, Planetary Missions Division. Doc: VVX-LES-IC-2269, Issue 1.6.

Esposito, L.W., Bertaux, J.L., Krasnopolsky, V., Moroz, V.I., Zasova, L.V., 1997. Chemistry of Lower Atmosphere and Clouds, in: Venus II: Geology, Geophysics, Atmosphere, and Solar Wind Environment. Univeristy of Arizona Press, p. 415.

Esposito, L.W., Knollenberg, R.G., Marov, M.I., Toon, O.B., Turco, R.P., 1983. The clouds and hazes of Venus, in: Venus. University of Arizona Press. chapter 16, pp. 484–564.

Gao, P., Zhang, X., Crisp, D., Bardeen, C.G., Yung, Y.L., 2014. Bimodal distribution of sulfuric acid aerosols in the upper haze of Venus. Icarus 231, 83–98. doi:10.1016/j.icarus.2013.10.013.

Grassi, D., Drossart, P., Piccioni, G., Ignatiev, N.I., Zasova, L.V., Adriani, A., Moriconi, M.L., Irwin, P.G.J., Negrão, A., Migliorini, A., 2008. Retrieval of air temperature profiles in the Venusian mesosphere from VIRTIS-M data: Description and validation of algorithms. J. Geophys. Res. Planets 113. doi:10.1029/2008JE003075.

Grassi, D., Politi, R., Ignatiev, N.I., Plainaki, C., Lebonnois, S., Wolkenberg, P., Montabone, L., Migliorini, A., Piccioni, G., Drossart, P., 2014. The Venus nighttime atmosphere as observed by the VIRTIS-M instrument. Average fields from the complete infrared data set. J. Geophys. Res. Planets 119, 837–849. doi:10.1002/2013JE004586.

Grieger, B., Ignatiev, N., Hoekzema, N., Keller, H.U., 2003. Indication of a Near Surface Cloud Layer on Venus from Reanalysis of Venera 13/14 Spectrophotometer Data, in: AAS/Division for Planetary Sciences Meeting Abstracts #35, p. 1487.

Grinspoon, D.H., Pollack, J.B., Sitton, B.R., Carlson, R.W., Kamp, L.W., Baines, K.H., Encrenaz, T., Taylor, F.W., 1993. Probing Venus's cloud structure with Galileo NIMS. Planet. Space Sci. 41, 515–542. doi:10.1016/0032-0633(93)90034-Y.

Hansen, J.E., Hovenier, J.W., 1974. Interpretation of the Polarization of Venus. J. Atmos. Sci. 31, 1137–1160. doi:10.1175/1520-0469(1974)031<1137:IOTPOV>2.0.CO;2.

Hashimoto, G.L., Sugita, S., 2003. On observing the compositional variability

of the surface of Venus using nightside near-infrared thermal radiation. J. Geophys. Res. Planets 108. doi:10.1029/2003JE002082.

Haus, R., Arnold, G., 2010. Radiative transfer in the atmosphere of Venus and application to surface emissivity retrieval from VIRTIS/VEX measurements. Planet. Space Sci. 58, 1578–1598. doi:10.1016/j.pss.2010.08.001.

Haus, R., Kappel, D., Arnold, G., 2013. Self-consistent retrieval of temperature profiles and cloud structure in the northern hemisphere of Venus using VIRTIS/VEX and PMV/VENERA-15 radiation measurements. Planet. Space Sci. 89, 77–101. doi:10.1016/j.pss.2013.09.020.

Haus, R., Kappel, D., Arnold, G., 2014. Atmospheric thermal structure and cloud features in the southern hemisphere of Venus as retrieved from VIRTIS/VEX radiation measurements. Icarus 232, 232–248. doi:10.1016/j.icarus.2014.01.020.

Hoffman, J.H., Hodges, R.R., Donahue, T.M., McElroy, M.M., 1980. Composition of the Venus lower atmosphere from the Pioneer Venus mass spectrometer. J. Geophys. Res. 85, 7882–7890. doi:10.1029/JA085iA13p07882.

Ignatiev, N., Grassi, D., Zasova, L., 2005. Planetary Fourier spectrometer data analysis: Fast radiative transfer models. Planet. Space Sci. 53, 1035–1042. doi:10.1016/j.pss.2004.12.009.

Ignatiev, N.I., Titov, D.V., Piccioni, G., Drossart, P., Markiewicz, W.J., Cottini, V., Roatsch, T., Almeida, M., Manoel, N., 2009. Altimetry of the

Venus cloud tops from the Venus Express observations. J. Geophys. Res. Planets 114. doi:10.1029/2008JE003320.

Imamura, T., Hashimoto, G.L., 2001. Microphysics of Venusian clouds in rising tropical air. J. Atmos. Sci. 58, 3597–3612. doi:10.1175/1520-0469(2001)058<3597:MOVCIR>2.0.CO;2.

James, E., Toon, O., Schubert, G., 1997. A Numerical Microphysical Model of the Condensational Venus Cloud. Icarus 129, 147–171. doi:10.1006/icar.1997.5763.

Kalashnikova, O., Horányi, M., Thomas, G.E., Toon, O.B., 2000. Meteoric smoke production in the atmosphere. Geophys. Res. Lett. 27, 3293–3296. doi:10.1029/1999GL011338.

Kawabata, K., Coffeen, D.L., Hansen, J.E., Lane, W.A., Sato, M., Travis, L.D., 1980. Cloud and haze properties from Pioneer Venus polarimetry. J. Geophys. Res. Space Phys. 85, 8129–8140. doi:10.1029/JA085iA13p08129.

Kliore, A.J., Moroz, V.I., Keating, G.M., 1985. The Venus International Reference Atmosphere. Adv. Space Res. 5.

Knollenberg, R.G., Hunten, D.M., 1980. The microphysics of the clouds of Venus: Results of the Pioneer Venus Particle Size Spectrometer Experiment. J. Geophys. Res. Space Phys. 85, 8039–8058. doi:10.1029/JA085iA13p08039.

Krasnopolsky, V.A., 2012. A photochemical model for the Venus atmosphere at 47–112 km. Icarus 218, 230–246. doi:10.1016/j.icarus.2011.11.012.

Krasnopolsky, V.A., 2015. Vertical profiles of H_2O, H_2SO_4, and sulfuric acid concentration at 45-75 km on Venus. Icarus 252, 327–333. doi:10.1016/j.icarus.2015.01.024.

Krasnopolsky, V.A., Pollack, J.B., 1994. H2O-H2SO4 system in Venus' clouds and OCS, CO, and H2SO4 profiles in Venus' troposphere. Icarus 109, 58–78. doi:10.1006/icar.1994.1077.

Kuntz, M., 1997. A new implementation of the Humlicek algorithm for the calculation of the Voigt profile function. J. Quant. Spectrosc. Radiat. Transfer 57, 819–824. doi:10.1016/S0022-4073(96)00162-8.

Lee, Y.J., Titov, D.V., Tellmann, S., Piccialli, A., Ignatiev, N., Pätzold, M., Häusler, B., Piccioni, G., Drossart, P., 2012. Vertical structure of the Venus cloud top from the VeRa and VIRTIS observations onboard Venus Express. Icarus 217, 599–609. doi:10.1016/j.icarus.2011.07.001.

Luginin, M., Belyaev, D., Fedorova, A., Vandaele, A.C., Montmessin, F., Korablev, O., Wilquet, V., Bertaux, J.L., 2014. Particles size distribution in the upper haze of Venus from SPICAV IR data, in: 40th COSPAR Scientific Assembly.

Maiorov, B., Ignat'ev, N., Moroz, V., Zasova, L., Moshkin, B., Khatuntsev, I., Ekonomov, A., 2005. A New Analysis of the Spectra Obtained by the Venera Missions in the Venusian Atmosphere. I. The Analysis of the Data Received from the Venera-11 Probe at Altitudes Below 37 km in the 0.44-0.66 μm Wavelength Range. Solar Syst. Res. 39, 267–282. doi:10.1007/s11208-005-0042-1.

Markiewicz, W.J., Titov, D.V., Limaye, S.S., Keller, H.U., Ignatiev, N., Jaumann, R., Thomas, N., Michalik, H., Moissl, R., Russo, P., 2007. Morphology and dynamics of the upper cloud layer of venus. Nature 450, 633–636. doi:10.1038/nature06320.

Mayer, B., Kylling, A., 2005. Technical note: The libRadtran software package for radiative transfer calculations - description and examples of use. Atmos. Chem. Phys. 5, 1855–1877. doi:10.5194/acp-5-1855-2005.

Mills, F.P., Esposito, L.W., Yung, Y.L., 2007. Atmospheric Composition, Chemistry, and Clouds, in: Exploring Venus as a Terrestrial Planet. American Geophysical Union, pp. 73–100. doi:10.1029/176GM06.

Moroz, V.I., Zasova, L.V., 1997. VIRA-2: a review of inputs for updating the Venus International Reference Atmosphere. Adv. Space Res. 19, 1191–1201. doi:10.1016/S0273-1177(97)00270-6.

Palmer, K.F., Williams, D., 1975. Optical Constants of Sulfuric Acid; Application to the Clouds of Venus? Appl. Opt. 14, 208–219. doi:10.1364/AO.14.000208.

Peña, O., Pal, U., 2009. Scattering of electromagnetic radiation by a multilayered sphere. Comput. Phys. Commun. 180, 2348–2354. doi:10.1016/j.cpc.2009.07.010.

Piccioni, G., Drossart, P., Sanchez-Lavega, a., Hueso, R., Taylor, F.W., Wilson, C.F., Grassi, D., Zasova, L., Moriconi, M., Adriani, a., Lebonnois, S., Coradini, a., Bézard, B., Angrilli, F., Arnold, G., Baines, K.H., Bellucci, G., Benkhoff, J., Bibring, J.P., Blanco, a., Blecka, M.I., Carlson, R.W., Di

Lellis, a., Encrenaz, T., Erard, S., Fonti, S., Formisano, V., Fouchet, T., Garcia, R., Haus, R., Helbert, J., Ignatiev, N.I., Irwin, P.G.J., Langevin, Y., Lopez-Valverde, M.a., Luz, D., Marinangeli, L., Orofino, V., Rodin, a.V., Roos-Serote, M.C., Saggin, B., Stam, D.M., Titov, D., Visconti, G., Zambelli, M., Ammannito, E., Barbis, A., Berlin, R., Bettanini, C., Boccaccini, A., Bonnello, G., Bouye, M., Capaccioni, F., Moinelo, A.C., Carraro, F., Cherubini, G., Cosi, M., Dami, M., De Nino, M., Del Vento, D., Di Giampietro, M., Donati, A., Dupuis, O., Espinasse, S., Fabbri, A., Fave, A., Veltroni, I.F., Filacchione, G., Garceran, K., Ghomchi, Y., Giustini, M., Gondet, B., Hello, Y., Henry, F., Hofer, S., Huntzinger, G., Kachlicki, J., Knoll, R., Driss, K., Mazzoni, A., Melchiorri, R., Mondello, G., Monti, F., Neumann, C., Nuccilli, F., Parisot, J., Pasqui, C., Perferi, S., Peter, G., Piacentino, A., Pompei, C., Reess, J.M., Rivet, J.P., Romano, A., Russ, N., Santoni, M., Scarpelli, A., Semery, A., Soufflot, A., Stefanovitch, D., Suetta, E., Tarchi, F., Tonetti, N., Tosi, F., Ulmer, B., 2007. South-polar features on Venus similar to those near the north pole. Nature 450, 637–640. URL: `http://www.scopus.com/inward/record.url?eid=2-s2.0-36749055721{&}partnerID=40{&}md5=eb328b2525df55435ccbb6dfc161d14a`, doi:`10.1038/nature06209`.

Piccioni, G., Drossart, P., Suetta, E., Cosi, M., Amannito, E., Barbis, A., Berlin, R., Bocaccini, A., Bonello, G., Bouyé, M., Capaccioni, F., Cherubini, G., Dami, M., Dupuis, O., Fave, A., Filacchione, G., Hello, Y., Henry, F., Hofer, S., Huntzinger, G., Melchiorri, R., Parisot, J., Pasqui, C., Peter, G., Pompei, C., Rèess, J.M., Semery, A., Soufflot, A., Adriani, A., Angrilli, F., Arnold, G., Baines, K., Bellucci, G., Benkhoff, J., Bezard, B., Bibring,

J.P., Blanco, A., Blecka, M.I., Carlson, R., Coradini, A., Di Lellis, A., Encrenaz, T., Erard, S., Fonti, S., Formisano, V., Fouchet, T., Garcia, R., Haus, R., Helbert, J., Ignatiev, N.I., Irwin, P., Langevin, Y., Lebonnois, S., Lopez Valverde, M.A., Luz, D., Marinangeli, M., Orofino, V., Rodin, A.V., Roos-Serote, M.C., Saggin, B., Sanchez-Lavega, A., Stam, B.M., Taylor, F., Titov, D., Visconti, G., Zambelli, M., 2007. VIRTIS: The Visible and Infrared Thermal Imaging Spectrometer. ESA Special Publication SP 1295.

Pollack, J.B., Dalton, J., Grinspoon, D., Wattson, R.B., Freedman, R., Crisp, D., Allen, D.A., Bézard, B., DeBergh, C., Giver, L.P., Ma, Q., Tipping, R., 1993. Near-Infrared Light from Venus' Nightside: A Spectroscopic Analysis. Icarus 103, 1–42. doi:10.1006/icar.1993.1055.

Rothman, L., Gordon, I., Babikov, Y., Barbe, A., Benner, D.C., Bernath, P., Birk, M., Bizzocchi, L., Boudon, V., Brown, L., Campargue, A., Chance, K., Cohen, E., Coudert, L., Devi, V., Drouin, B., Fayt, A., Flaud, J.M., Gamache, R., Harrison, J., Hartmann, J.M., Hill, C., Hodges, J., Jacquemart, D., Jolly, A., Lamouroux, J., Roy, R.L., Li, G., Long, D., Lyulin, O., Mackie, C., Massie, S., Mikhailenko, S., Müller, H., Naumenko, O., Nikitin, A., Orphal, J., Perevalov, V., Perrin, A., Polovtseva, E., Richard, C., Smith, M., Starikova, E., Sung, K., Tashkun, S., Tennyson, J., Toon, G., Tyuterev, V., Wagner, G., 2013. The HITRAN 2012 molecular spectroscopic database. J. Quant. Spectrosc. Radiat. Transfer 130, 4–50. doi:10.1016/j.jqsrt.2013.07.002.

Rothman, L., Gordon, I., Barber, R., Dothe, H., Gamache, R., Goldman,

A., Perevalov, V., Tashkun, S., Tennyson, J., 2010. HITEMP, the high-temperature molecular spectroscopic database. J. Quant. Spectrosc. Radiat. Transfer 111, 2139 – 2150. doi:10.1016/j.jqsrt.2010.05.001.

Satoh, T., Ohtsuki, S., Iwagami, N., Ueno, M., Uemizu, K., Suzuki, M., Hashimoto, G.L., Sakanoi, T., Kasaba, Y., Nakamura, R., Imamura, T., Nakamura, M., Fukuhara, T., Yamazaki, A., Yamada, M., 2015. Venus' clouds as inferred from the phase curves acquired by IR1 and IR2 on board Akatsuki. Icarus 248, 213–220. doi:10.1016/j.icarus.2014.10.030.

Seiff, A., Schofield, J., Kliore, A., Taylor, F., Limaye, S., Revercomb, H., Sromovsky, L., Kerzhanovich, V., Moroz, V., Marov, M., 1985. Models of the structure of the atmosphere of Venus from the surface to 100 kilometers altitude. Adv. Space Res. 5, 3–58. doi:10.1016/0273-1177(85)90197-8.

Shalygina, O.S., Petrova, E.V., Markiewicz, W.J., Ignatiev, N.I., Shalygin, E.V., 2015. Optical properties of the Venus upper clouds from the data obtained by Venus Monitoring Camera on-board the Venus Express. Planet. Space Sci. 113, 135–158. doi:10.1016/j.pss.2014.11.012.

Stamnes, K., Tsay, S.C., Wiscombe, W., Jayaweera, K., 1988. Numerically stable algorithm for discrete-ordinate-method radiative transfer in multiple scattering and emitting layered media. Appl. Opt. 27, 2502–2509. doi:10.1364/AO.27.002502.

Stamnes, K., Tsay, S.C., Wiscombe, W., Laszlo, I., 2000. DISORT, a General-Purpose Fortran Program for Discrete-Ordinate-Method Radiative Transfer in Scattering and Emitting Layered Media: Documentation of

Methodology. Technical Report. Dept. of Physics and Engineering Physics Stevens Institute of Technology Hoboken, NJ 07030.

Tonkov, M.V., Filippov, N.N., Bertsev, V.V., Bouanich, J.P., Van-Thanh, N., Brodbeck, C., Hartmann, J.M., Boulet, C., Thibault, F., Doucen, R.L., 1996. Measurements and empirical modeling of pure CO_2 absorption in the 2.3-μm region at room temperature: far wings, allowed and collision-induced bands. Appl. Opt. 35, 4863–4870. doi:10.1364/AO.35.004863.

Tran, H., Boulet, C., Stefani, S., Snels, M., Piccioni, G., 2011. Measurements and modelling of high pressure pure CO_2 spectra from 750 to 8500 cm^{-1}. I–central and wing regions of the allowed vibrational bands. J. Quant. Spectrosc. Radiat. Transfer 112, 925–936. doi:10.1016/j.jqsrt.2010.11.021.

Tsang, C., Irwin, P., Taylor, F., Wilson, C., 2008. A correlated-k model of radiative transfer in the near-infrared windows of Venus. J. Quant. Spectrosc. Radiat. Transfer 109, 1118–1135. doi:10.1016/j.jqsrt.2007.12.008.

Wilquet, V., Drummond, R., Mahieux, A., Robert, S., Vandaele, A.C., Bertaux, J.L., 2012. Optical extinction due to aerosols in the upper haze of Venus: Four years of SOIR/VEX observations from 2006 to 2010. Icarus 217, 875–881. doi:10.1016/j.icarus.2011.11.002.

Wilquet, V., Fedorova, A., Montmessin, F., Drummond, R., Mahieux, A., Vandaele, A.C., Villard, E., Korablev, O., Bertaux, J.L., 2009. Preliminary characterization of the upper haze by SPICAV/SOIR solar occultation in

UV to mid-IR onboard Venus Express. J. Geophys. Res. Planets 114. doi:10.1029/2008JE003186.

Wilson, C.F., Guerlet, S., Irwin, P.G.J., Tsang, C.C.C., Taylor, F.W., Carlson, R.W., Drossart, P., Piccioni, G., 2008. Evidence for anomalous cloud particles at the poles of Venus. J. Geophys. Res. Planets 113, E00B13. doi:10.1029/2008JE003108.

Zasova, L., 2012. Reference atmospheres: VIRA II -Venus International Reference Atmosphere update., in: 39th COSPAR Scientific Assembly, p. 2248.

Zasova, L., Ignatiev, N., Khatuntsev, I., Linkin, V., 2007. Structure of the Venus atmosphere. Planet. Space Sci. 55, 1712–1728. doi:10.1016/j.pss.2007.01.011.